Hybrid RANS/LES of Turbulent forced convection flow over tandem square cylinders

Kaveenraj H

A Thesis Submitted to
Indian Institute of Technology Hyderabad
In Partial Fulfillment of the Requirements for
The Degree of Master of Technology

भारतीय प्रौद्योगिकी संस्थान हैदराबाद
Indian Institute of Technology Hyderabad

Department of Mechanical and Aerospace Engineering

June 2019

Declaration

I declare that this written submission represents my ideas in my own words, and where ideas or words of others have been included, I have adequately cited and referenced the original sources. I also declare that I have adhered to all principles of academic honesty and integrity and have not misrepresented or fabricated or falsified any idea/data/fact/source in my submission. I understand that any violation of the above will be a cause for disciplinary action by the Institute and can also evoke penal action from the sources that have thus not been properly cited, or from whom proper permission has not been taken when needed.

(Signature)

Kaveenraj·H

(Kaveenraj H)

ME17MTECH11005

(Roll No.)

Approval Sheet

This Thesis entitled Hybrid RANS/LES of Turbulent forced convection flow over tandem square cylinders by Kaveenraj H is approved for the degree of Master of Technology from IIT Hyderabad
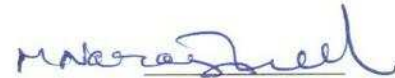
(Dr.Narasimha Mangadoddy)External examiner
Dept. of Chemical Engineering
IITH

(Dr.Pankaj Sharadchandra Kolhe)Internal examiner
Dept.of Mechanical and Aerospace Engineering
IITH

(Dr.Venkatasubbaiah K) Adviser
Dept. of Mechanical and Aerospace Engineering
IITH

(Dr.Narasimha Mangadoddy) Chairman
Dept. of Chemical Engineering
IITH

Acknowledgements

Dedication

To myself and to my beloved family

Abstract

Heat transfer in a turbulent forced convection flow over a tandem square cylinder has been numerically studied at moderate Reynolds numbers. The effects of complex wake interactions behind the cylinder on heat transfer is studied. Turbulence is modelled by Detached Eddy Simulation (DES) with kOmegaSSTDES and SpalartAllmarasDES model available in OpenFOAM solver. The forced convection flow is formulated by two dimensional unsteady incompressible flow by neglecting buoyancy terms. The flow domain dimensions have been chosen such that the blockage ratio is less than 5%. The governing equations are solved numerically by Finite Volume method. Results are reported for different Reynolds numbers by varying spacings between the 2 cylinders from 2D to 5D, varying configuration and varying sizes of cylinders. The velocity and vorticity profiles and average Nusselt number values for both the cylinders are presented. The wake region behind the cylinders varies significantly with spacing between the cylinders affecting the heat transfer characteristics of downstream cylinder. The effect of Reynolds number in heat transfer characteristics is less pronounced in the second cylinder as compared to the first cylinder. The present results are matching well with the available experimental correlations and results available in the literature.

Contents

List of Figures

List of Tables

Nomenclature

D Size of the square cylinder (m)

S Distance between square cylinder (m)

μ_t Turbulent viscosity

k mean turbulent energy per unit mass (m^2/s^2)

U Velocity (m/s)

T Temperature (K)

ω Turbulent frequency

ϵ Turbulent dissipation rate

$\delta_x; \delta_y; \delta_z$ Mesh size in x, y and z direction

Δ filter width

$G(x)$ filter function

S   Strain invariant

S_{ij} Strain rate tensor

C_s Smagorinsky constant

C_{b1}, C_{w1} Smagorinsjy model constant

d   Turbulent length scale (m)

y_w near wall distance

C_{DES} DES model constant

$l_{k-\omega}$ k-omega SST length scale

$\tilde{l}$ DES turbulence length scale

F_1 Blending Function

SGS   Subgrid scale

SST   Shear Stress Transport

RANS   Reynolds Average Navier Stoke

Chapter 1

Introduction

Bluff bodies can be found in many engineering applications, such as bridges, tall buildings and towers, maritime vessels, road and rail based vehicles and in various aeronautical applications. A bluff body has a non-streamlined geometry that produces significant resistance when immersed in a moving fluid. Separation occurs over a large section of a bluff body, which produces a high pressure drag force and a large wake region. Bluff body wakes have been the subject of extensive investigation in view of their applications to wind engineering, hydrodynamics, aerodynamics and electronics cooling also. Such wakes display characteristics that are distinct to the object shape, Reynolds number and distance from the object itself. At high Reynolds numbers, the wake structure is complex owing to unsteadiness and turbulence. In the lower range of the Reynolds number, recent studies show that the flow field, along with unsteadiness, is complex owing to three dimensionality even in nominally two dimensional geometries. Bluff body cross section that are often employed are circular and rectangular (especially, square). Usually, the bluff bodies (representative of a specific system or equipment) are of different sizes and have complex shapes. They can be placed in the wake of other bodies, leading to either an increase or a decrease of their cooling. An application of such flows is found in aeronautical engine compartments where the thermal behaviour of equipment like valves, electrical harnesses, or ducts have to be studied in order to guarantee that they never exceed their maximum allowable temperature in the whole aircrafts flight envelope. The most striking phenomenon in flows past multiple bluff bodies is the generation of a complex structure by the mutual interactions among the wakes behind the bodies. These wake interactions subsequently lead to vortex shedding. Heat transfer and the resulting thermal field is controlled by this complex unsteady flow. Let us try to understand the flow over single and multiple circular cylinders and then focus on flow over square cylinders.

1.1   Flow over bluff bodies

The flow around bluff bodies are defined by four regions of disturbances.

- A narrow region of deaccelerated flow before the cylinder where the flow hits the front region of the cylinder in the stagnation point. Whose mean velocity is that of free stream velocity.

- Development of boundary layers close to the surface of the cylinder formed due to positive pressure gradient.

- Regions of disturbed flow over and below the cylinder due to blockage caused by the objects which leads to acceleration and displacement of fluid.

- The appearance of a wide region of separated flow known as wake downstream of the cylinder which is affected by the state of the flow.
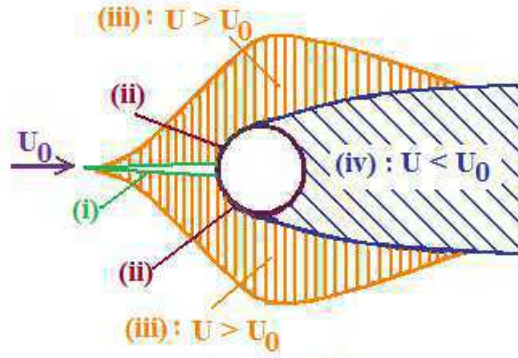
Figure 1.1: Regions of disturbed flow around a cylinder[1]

To be able to model the complex flow around different geometries we must consider the rotationality and viscosity of the flow.

1.1.1 Turbulence flow

The downstream region of cylinder characterizes various flow regimes depending on the Reynolds number ranging from small to large Reynolds number. The wake formation length increases with Re in the laminar steady regime, followed by a decrease in the laminar vortex shedding and an increase beyond the 3D wake transition regime. Where, the Reynolds number is defined with free stream velocity, U and cylinder diameter, D.

$$Re = \frac{\rho U D}{\mu} \tag{1.1}$$

Where ρ, is the density and μ, is the dynamic viscosity of the fluid. At $Re = 180$, the periodic Strouhal wake transitions from two-dimensional to a three dimensionality causing laminar periodic wake to become unstable from observations of Roshko[3]. Further confirmed by Karniadakis and Trianttafyllou [4], who showed that at a Reynolds number of 200 formation of secondary instable structures in the two-dimensional vortex street lead to three dimensional wake region. There are two types of regimes involved in turbulent flows.

- **Critical regime** In this regime the cylinder boundary layer becomes turbulent and wake becomes narrow and disorganized. Bearman[5] observed the transition of flow from laminar to turbulent separation of boundary for $2 \times 10^5 \leq Re \leq 4 \times 10^5$ using hot wire probe in the wake region.

- **Postcritical regime** In this regime the regular vortex shedding is re-established with a turbulent boundary layer. The separation point is displaced towards the rear end of the cylinder[6]

2
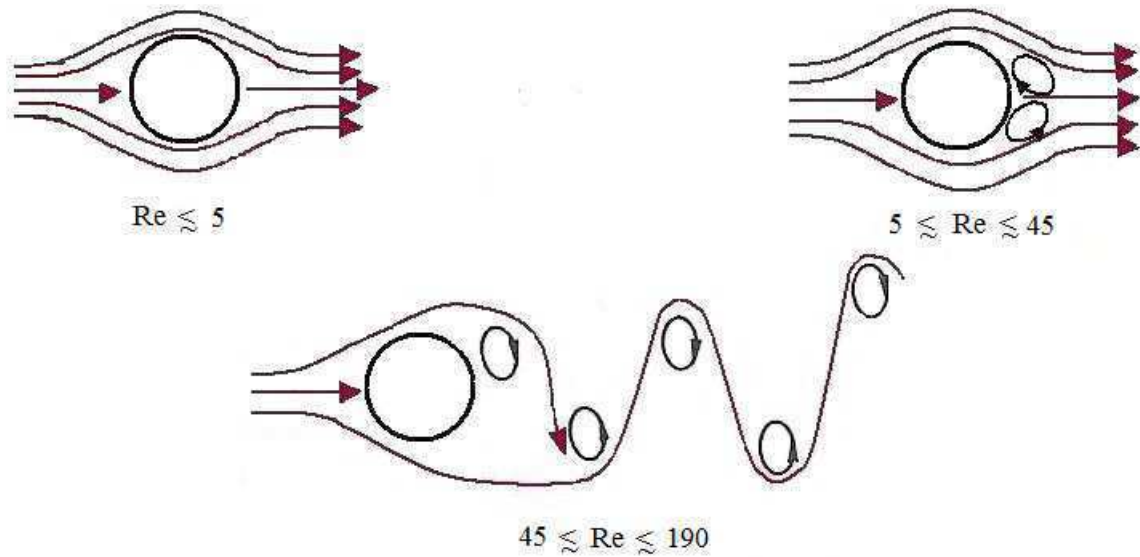
Figure 1.2: Flow pattern for a circular cylinder in laminar cross flow
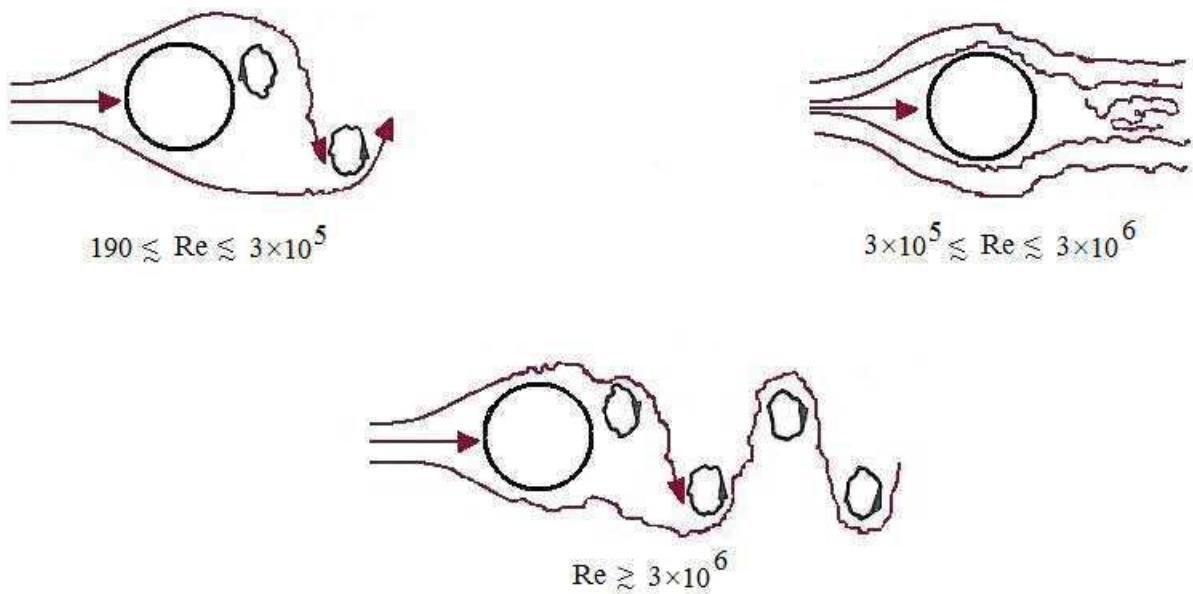
Figure 1.3: Flow pattern for a circular cylinder in turbulent cross flow[2]

1.2 Flow over multiple bodies

The flow pattern over tandem circular and square cylinder are similar. When two circular cylinders are subjected to a steady flow, the resulting forces and flow pattern in the wake may be very different from those found on a single cylinder at the same Reynolds number. The fluid flow behaviour around two circular cylinders depends on the spacing between the cylinders, the orientation of

the cylinders relative to the oncoming flow, Reynolds number, surface roughness, and free-stream turbulence. Two circular cylinders of equal diameter, D, can be classified in three basic categories of possible arrangements based on the angle between the centre connection line of the cylinders.The spacing is typically expressed as dimensionless longitudinal and transverse pitch ratios, L/D and T/D, respectively

- **Tandem arrangement** An arrangement in which the two cylinders are arranged one behind the other such that the angle α is $0\,\mathrm{deg}$
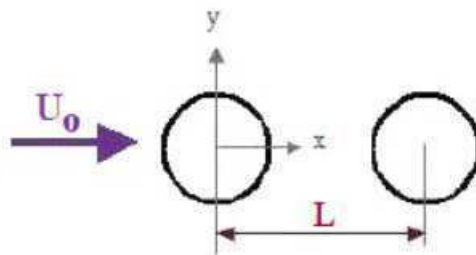
Figure 1.4: Tandem arrangement

- **Side by side arrangement** An arrangement where the cylinders in a way such that the angle α is $90\,\mathrm{deg}$
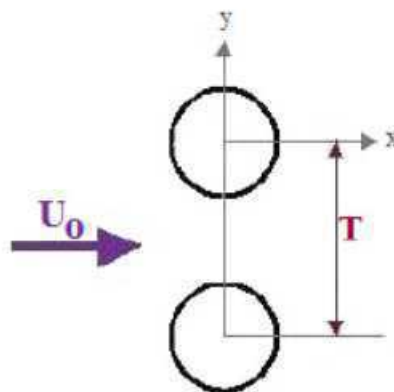
Figure 1.5: Side by side arrangement

- **Staggered arrangement** An arrangement where the angle of the cylinders are in between $0\,\mathrm{deg}$ and $90\,\mathrm{deg}$
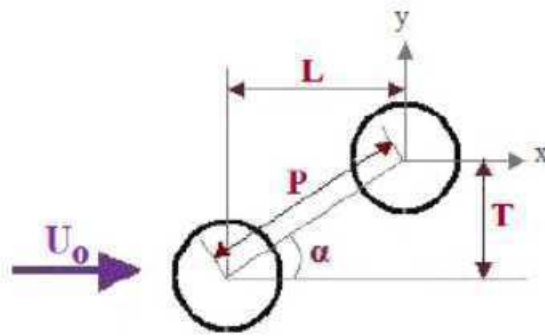
Figure 1.6: Staggered arrangement.

Flow pattern

The different types of interference will naturally induce different flow patterns around the tandem cylinders. These flow patterns will vary with spacing and Reynolds number, as the interference regions do. Igarashi[7] classified different flow patterns for different spacings and Reynolds numbers. This flow pattern is shown in figure 7. The figure are taken from Igarashi[7]
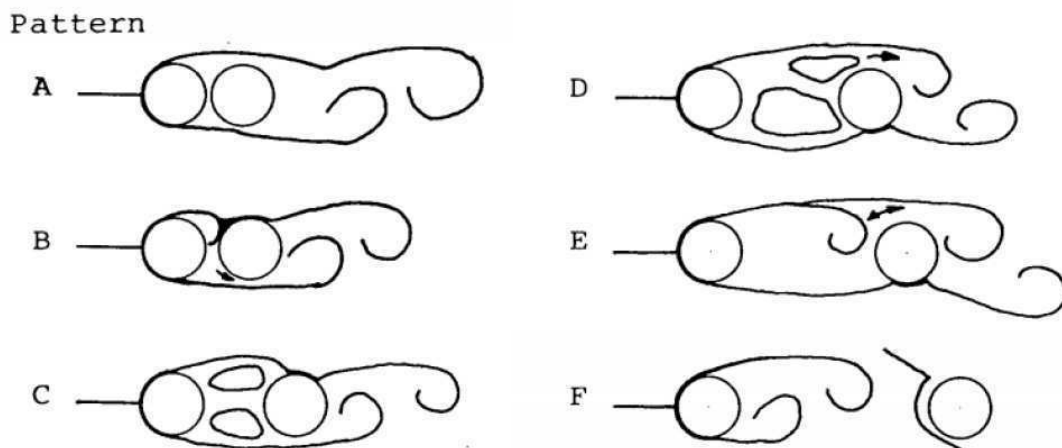
Figure 1.7: Different flow patterns for tandem cylinders.

For pattern A, the downstream cylinder is located inside the vortex formation region of the upstream cylinder and the free shear layers wrap around it. The shear layers become elongated compared to the ones of a single cylinder, the wake becomes narrower and vortex shedding happens for a higher Strouhal number.The reattachment region comprises patterns B, C, D, E, E and G,[8] . Here, the shear layer from the upstream cylinder can no longer enclose the downstream cylinder and they start to reattach to it instead. Eddies may form in the gap between the cylinders. The

gap flow is very complex and it has not yet been found a complete explanation of what happens in this region. In pattern B, there is a synchronization of reattachment of the upstream shear layer on the downstream cylinder and a vortex shed from the opposite side of the downstream cylinder. In pattern C, quasi-stationary eddies are formed in the gap and the reattachment is nearly continuous. When the spacing is increased, intermittent vortex shedding from the upstream cylinder can happen in the gap. This is pattern D in the classification of Igarashi[7]. In pattern F, there is vortex shedding from both cylinders. This happens as the critical spacing between the cylinder is reached. The vortices shed from the upstream cylinder impinges the downstream one and this triggers the vortex shedding of the downstream cylinder. This flow pattern is also called co-shedding because of this phenomena. The difference between a bi-stable flow and an unstable flow is that the flow picture of as unstable flow last only for a very short time before it changes, while that of a bi-stable flow has a certain duration.

1.3 Flow over square cylinder

The flow over a square cylinder also has the similar regimes of flow as that of circular cylinders with the regimes changing at different Reynolds number. The main difference is the location of separation point. The separation point in a square cylinder is fixed at the leading edge at the top and bottom of its surface because of its geometry as opposed to cylindrical where it changes with flow regimes. The difference in the nature of the flow separation results in significantly distinct features of the flow structures and fluid forces between the circular and square cylinder cases.[8][9][10][11] At $Re < 50$, the flow around a square cylinder is steady, characterized by a pair of counter-rotating recirculating bubbles downstream of the cylinder. No alternating von Karman vortex shedding occurs from the cylinder. At $Re > 50$, the unsteady laminar flow occurs, with the alternating von Karman vortex shedding from the cylinder. The unsteady flow separates from the trailing corners of the square cylinder at $Re < 120$ but from the leading corners at $Re > 120$ [12][13]. At this $Re_{c2} = 150$, the so called mode A instability and the transition from $2D$ to $3D$ flows occur. Mode A is featured by spanwise vortex dislocation, streamwise vortex loops, and a relatively large spanwise wavelength (around $5.2D$) of the streamwise vortices[14, 15] . With a further increase in Re, the so-called mode B instability is identified at another critical Reynolds number $Re_{c2} = 190250$, which is again dependent on the factors such as turbulence intensity, blockage, and aspect ratio. In mode B, the spanwise wavelength of the streamwise vortices is much smaller, around $1.2D$, than that in mode A. The flow around the square cylinder becomes turbulent at $Re > Re_{c2}$.

1.4 Literature survey

Lyn and Rodi[16] did a experimental study of the turbulent shear layer and the associated recirculation region on the sidewall formed in flow separation from the forward corner of a square cylinder with one-component laser-Doppler velocimetry. He found that due to vortex shedding the flow was approximately periodic and the shear layer separating from a front edge of a square cylinder shares features with both forced and unforced mixing layers, with steady separated flow with recirculation, as well as with forced separated boundary layers.

Brun et al.[17] studied various time scales of the turbulent separating flow around a square

cylinder with Unsteady analysis based on large eddy simulation (LES) at intermediate Reynolds numbers($Re < 20000$) and laser doppler velocimetry (LDV) measurements at high Reynolds number($Re > 20000$) with Reynolds number is ranging from $Re = 50$ to $Re = 300,000$. For Reynolds number range above $Re \approx 1000$, both signatures of Von Karman (VK) and KelvinHelmholtz (KH) type vortical structures are found on velocity time samples. The occurrence of KH pairings in the separating shear layer on the side of the cylinder and confirm the intermittency nature of such a shear flow similar to round cylinder case was observed.

A coupled experimental/numerical analysis of turbulent flow past a square cylinder is performed at the ERCOFTAC Reynolds number $Re = \frac{\rho U D}{\mu} = 21,400$, where U is the inflow velocity and D the cylinder height. Minguez et al.[18]using Laser Doppler Velocimetry (LDV) and high-order large-eddy simulations (LES) approaches. SVV-LES results capture numerically in turbulent regime the high frequency range related to the KH instability and flow is found to separate at the leading edge of the cylinder with the occurence of three-dimensional KelvinHelmholtz (KH) pairings localized in the separating shear layer.

Cao and Tamura[19] studied the flow past a square cylinder at Reynolds number of $Re = 22000$ using large eddy simulation(LES) with the open-source finite volume method code ($OpenFOAM 2.3.0$) with $1st 2nd$ order schemes is applied for unstructured LES. He found that OpenFOAM can obtain fairly accurate prediction of the time-averaged and r.m.s quantities no matter which numerical scheme is used and the KelvinHelmholtz instability can be accurately predicted.

Igarashi[20] carried out an experimental investigations of heat transfer from a single square prism to an air stream in the ranger of sub-critical Reynolds number in the range $5.6 x 10^3 < Re < 5.6 x 10^4$. He found that there was no difference in average heat transfer coefficient for constant wall temperature and constant heat flux conditions and heat transfer coefficients increases directly with increases in the values of the reciprocal of the length of vortex formation region. He also carried out investigations local heat transfer from a square prism at angle of attack to an airstream at Reynolds number range $1.1 x 10^4 C Re < 5.3 x 10^4$[21]. The heat transfer coefficients in the reattachment region were examined and each sides had different heat transfer rates.

Flow over two inline square cylinders have also been characterized in the last two decades. Sakamoto et al.[22] observed significant changes in the time-mean and fluctuating forces acting on the cylinders for spacing ratios above and below the critical value $L/D = 4$ at $Re = 27600$ and 55200 for two square prisms in a tandem arrangement situated in uniform flow using experimental investigations. These changes were associated with different flow patterns; namely, the regular shedding of vortices from the upstream cylinder was suppressed for $L/d < 4$ and periodical vortex shedding from each of the cylinders beginning at the critical spacing $L/D = 4$. At the critical spacing, the time-mean drag and fluctuating lift and drag acting on the two cylinders were found to jump discontinuously to reach their maximum values.

This paper reports an experimental investigation of flow over a square cylinders[23]. When the two cylinders were in tandem formation, a critical spacing equal to about four times the side length D of the square cylinder, was found to exist. For $L/D < (L/D)_{cri}$, where L is the streamwise centre to centre spacing between the two cylinders, the boundary layers which separate from the upstream cylinder reattach onto the downstream cylinder and only the latter sheds vortices.When the two cylinders were in staggered formation an unstable regime exists at $4 \leq L/D \leq 12$.

This paper reports an experimental study on the flow characteristics around two square cylinders

in a tandem arrangement. The spacing between the centers of the cylinders ranges from 1.5 to 9 widths of the cylinder and the Reynolds number ranges from 2.0×10^3 to 1.6×10^4. Hysteresis with two discontinuous jumps is present for all the Reynolds numbers studied when the spacing is varied in two different ways, one being a progressive increase and the other a progressive decrease. The hysteresis is associated with two different flow patterns, and the discontinuity is attributed to a sudden change of the flow pattern. In the hysteresis regime, only one flow pattern is stable, differing from the bistable phenomenon that involves intermittent switching between two stable flow patterns as reported for higher Reynolds numbers[24].

Flow fields around two square cylinders in a tandem arrangement were investigated using particle image velocimetry (PIV)[25]. The experiments were made for the spacing between the two cylinders ranging from $s/D = 0.5 to 10.0$ and two Reynolds numbers of $5,300$ and $16,000$. The results showed that the flow patterns at $s/D = 2.0$ were drastically different from those at $s/D = 2.5$ for both Reynolds numbers. The sudden change in the flow patterns depended on the reattachment of the shear layer separated from the upstream cylinder. At $Re = 5,300$, the separated shear layers at both upstream corners of the upstream cylinder met at the front face of the downstream cylinder. However, at $Re = 16,000$, the separated shear layers met farther upstream near $x/D = 2.5$.

Tatsutani et al.[26] studied incompressible, two- dimensional, unsteady flow and heat transfer past a pair of cylinders of square cross section using dye visualization and direct numerical simulation, placed in tandem normal to the flow in a channel at $200 < Re < 1600$ for varying spacings from $L/D = 0.2 to 4$. The optimal spacing for the upstream cylinder was found to be smaller than the critical separation and also the temperature of the upstream surface is relatively insensitive to the different inter-cylinder spacings. The temperatures of the top and bottom surfaces increase slightly with increasing inter-cylinder spacing.

Sohankar and Etminan[27] presented numerical study on the flow characteristics and heat transfer over two equal square cylinders in a tandem arrangement at Spacing of $5D$ and the Reynolds number ranging from 1 to 200. It is found that the Nusselt number for the front surface displays the highest value, the top and bottom surface value is intermediate, and the rear surface has the lowest value. The level of Nusselt number for the upstream cylinder is higher than the corresponding value for the downstream cylinder.

Rodi et al.[28] presented a short overview of LES, the subgrid scale models that are used in LES, the numerical methods used, results obtained for two complex flows, and an assessment of those results. They considered a flow over square cylinder and cube separately and compared the results. They found of the cases considered here, the cube flow was predicted much more accurately than the square cylinder flow. It appears that this is a consequence of the square cylinder flow having a transitional character and the possibility(which should be investigated) that this flow is much more sensitive to small changes in the controlling parameters. In general, it appears that transitional flows are more challenging than fully developed ones.

This paper presents large eddy simulation (LES) results of convective heat transfer and incompressible-fluid flow around a square cylinder (SC) at Reynolds numbers in the range from 10^3 to 3.5×10^5. The LES uses the swirling-strength based sub-grid scale (SbSGS) model. Several flow properties at turbulent regime are explored, including lift and drag coefficients, time-spanwise averaged sub-grid viscosity, and Kolmogorov micro-scale. Local and mean Nusselt numbers of convective heat transfer from the SC under isothermal wall temperature are predicted and compared with empirical

results[29].

Wiesche[30] did a LES study has been conducted for a flow past a heated square cylinder employing two computational grids for $Re = 22,000$. The LES method is a conventional one with the Smagorinsky eddy-viscosity model, and the computational grid is small enough to be handled by workstations. The computed turbulent flow field quantities agree well with the experimental results reported by Lyn et al. The computed values for the mean Nusselt number as function of the Reynolds number were in excellent agreements to the empirical correlations proposed by Hilpert or by Sparrow et al.

Roy and Barone[31] did simulations of a low-speed square cylinder wake and a supersonic axisymmetric base wake are performed using the Detached Eddy Simulation (DES) model. A reduced-dissipation scheme is demonstrated on a $2D$ square cylinder wake problem, showing a dramatic increase in accuracy for a given grid resolution. The results for simulations on three grids of increasing resolution for the 3D square cylinder wake are compared to experimental data and to other LES and DES studies. The comparisons of mean flow and global mean flow quantities to experimental data are favorable, while the results for second order statistics in the wake are mixed and do not always improve with increasing spatial resolution. Comparisons to LES studies are also generally favorable, suggesting DES provides an adequate subgrid scale model.

This paper presents a large eddy simulation (LES) of flow and heat transfer in a tandem configuration of two square cylinders at moderate Reynolds number ($Re = 16,000$) at spacing of $L/D = 4$[32]. Compressible LES on a hybrid mesh is used to predict the flow structure and the heat transfer at the wall. The wall adapting linear eddy model is chosen to model the subgrid turbulent viscosity. He observed that upstream cylinder almost behaved like a isolated cylinder and heat transfer coefficient of downstream cylinder was higher.

Flow passing a heated single square cylinder is investigated using a hybrid LES-RANS approach on unstructured grids at a moderate Reynolds number of $22,050$. The implicit sub-grid scale model is apply to LES, and two turbulence models, the Spalart-Allmaras model and the SST k-ω model, are employed for near-wall RANS. Combined with LES, both models present good predictions of the time- and phase-averaged velocity profiles on a 4-million-cell grid. Results of the LES-SST approach agree better with the experimental data especially at locations close to the cylinder surface and this leads to improved surface convective heat transfer compared to LES-SA[33].

1.5 Motivation

The turbulent flow characteristics over single and tandem square cylinder has been studied extensively. The literatures have given little focus on the heat transfer characteristics and very few available has also been done at lower Reynolds number. The effects spacings, sizes of cylinder and different configurations of square cylinders at moderate Reynolds number needs to be studied. And also Studies in the past have not dealt with using hybrid RANS/LES approach while numerically simulating turbulent flow over square cylinders. The forced convection heat transfer in such flows have also not been paid attention in high Reynolds number flows. The motivation lies in the prediction of data quantitatively as well as qualitatively so as to match available results using two different Hybrid RANS /LES approaches. Hybrid RANS /LES approach has been opted in order to have higher accuracy with lesser computational expense.

1.6 Objectives of the present study

The thesis involves the study of the effect of the first cylinder on the downstream cylinder and to analyse the heat transfer characteristics of both the cylinder. The major objectives of the present study is:

- Analyzing the capability of Hybrid RANS and LES(both k-ω SST and SA) solver for incompressible turbulent flow.

- To study the effects of the following on heat transfer of the cylinders.

    - Reynolds number

    - Spacing between the cylinder.

    - Different sizes of the cylinder.

- To study the difference in heat transfer between tandem and staggered configurations.

1.7 Thesis outline

Thesis is organized in the following manner,

- Chapter 1 had a brief introduction to circular and square cylinders. The literature survey explained the work that had been done on flow over square cylinders and what has to be done

- Chapter 2 covers the geometrical dimensions domain of flow, which is followed by the detailed formulation of different methods used for current study.

- Chapter 3 provides the validation of solver being used for flow over single and tandem square cylinders.

- Chapter 3 also covers results and discussions part of variation Reynolds number, spacing, sizes of cylinder and configurations in detail.

- Chapter 3 represents the conclusions made from validations and results obtained.

Chapter 2

Mathematical formulation with governing equations

2.1   Problem setup

To study the heat transfer characteristics using hybrid RANS/LES model in two-dimensional incompressible turbulent flow over tandem square cylinders with the medium air. The geometry details are taken from Duchaine et al.[32] The square has a side, s=D. Height of the domain is 15D, upstream length is 9D and the downstream length is 17D. The computational domain have been designed to make sure that the blockage ratio is less than 5% so that the flow over cylinder is not disturbed by the boundary layer formed over the bottom and top surfaces of the computational domain.
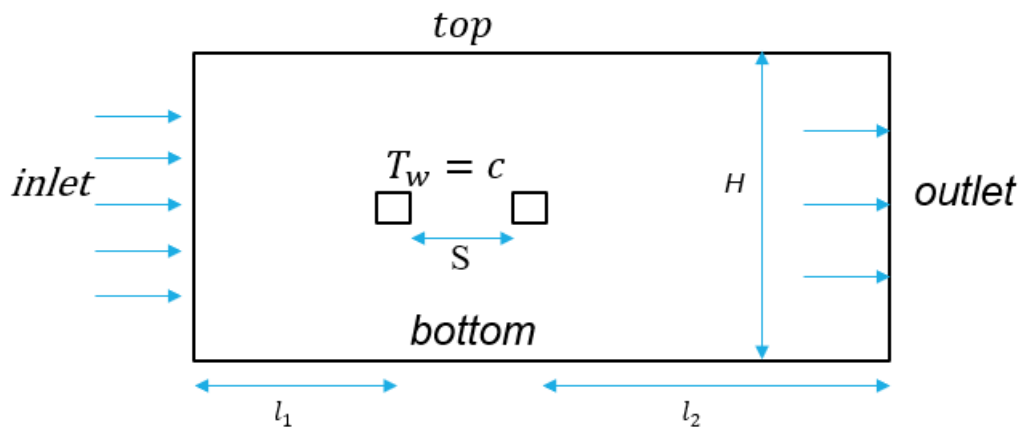

Figure 2.1: Computational domain of flow over tandem square cylinders at constant wall temperature

2.2   Governing equations

2.2.1   k-ω SST DES model

- **Navier Stokes equation.**

$$\frac{\partial}{\partial t}(u_i) + \frac{\partial}{\partial x_j}(u_i u_j) = -\frac{1}{\rho}\frac{\partial}{\partial x_j}(p) + \frac{\partial}{\partial x_j}\Big(\nu\frac{\partial}{\partial x_j}u_i\Big) \tag{2.1}$$

- **The turbulence specific dissipation rate equation.**

$$\frac{D}{Dt}(\rho\omega) = \nabla\cdot(\rho D_\omega\nabla\omega) + \rho\gamma\frac{G}{\nu} - \frac{2}{3}\rho\gamma\omega(\nabla\cdot\mathbf{u}) - \rho\beta\omega^2 - \rho(F_1 - 1)CD_{k\omega} + S_\omega \tag{2.2}$$

- **Turbulence kinetic energy**

$$\frac{D}{Dt}(\rho k) = \nabla\cdot(\rho D_k\nabla k) + min(\rho G, (c_1\beta^*)\rho k\omega) - \frac{2}{3}\rho k(\nabla\cdot\mathbf{u}) - \rho\frac{k^{1.5}}{\tilde{d}} + S_k \tag{2.3}$$

The length scale,$\tilde{d}$, is given by

$$min\Big(C_{DES}\Delta, \frac{\sqrt{k}}{\beta^*\omega}\Big) \tag{2.4}$$

The turbulence viscosity is obtained using:

$$\nu_t = a_1\frac{k}{max(a_1\omega, b_1 F_{23}\mathbf{S})} \tag{2.5}$$

2.2.2   Spalart-Allmaras DES

- **The $\tilde{\nu}$ transport equation**

$$\frac{D}{Dt}(\rho k) = \nabla\cdot(\rho D_{\tilde{\nu}}) + \frac{C_{b2}}{\sigma_{\nu_t}}\rho|\nabla\tilde{\nu}|^2 + C_{b1}\rho\tilde{S}\tilde{\nu}\Big(1 - f_{t2}\Big) - \Big(C_{w1}f_w - \frac{C_{b1}}{\kappa^2}f_{t2}\Big)\rho\frac{\tilde{\nu}^2}{\tilde{d}^2} + S_{\tilde{\nu}} \tag{2.6}$$

where the length scale $\tilde{d}$ is defined by,

$$min(\Psi C_{DES}\Delta, y) \tag{2.7}$$

where Ψ is the low Reynolds number correction function.

2.3   Boundary conditions

For the flow over tandem square cylinders the uniform velocity and temperature is specified at inlet of the channel.No slip boundary condition applied on the sides of the square, at the outlet section of the channel , the fully developed flow condition is assumed for both velocity and temperature fields. Free stream conditions are employed at the borrom and top domain surfaces and where the walls of the squares are applied with constant wall temperature.

- At the inlet horizontal uniform velocity and Temperature are specified.

$$u = u_0, T = T_0 \tag{2.8}$$

- On the top wall of the domain free stream temperature and horizontal velocity boundary conditions are applied.

$$u = u_0, v = 0, T = T_0 \tag{2.9}$$

- On the bottom wall of the domain free stream temperature and horizontal velocity boundary conditions are applied.

$$u = u_0, v = 0, T = T_0 \tag{2.10}$$

- In the outlet of the channel the fully developed flow boundary conditions is applied for both velocity and temperature fields.

$$\frac{\partial u}{\partial x} = 0, \frac{\partial T}{\partial x} = 0 \tag{2.11}$$

- On the surfaces of the cylinder constant wall temperature and no slip boundary conditions are applied

$$T = T_w, u = 0, v = 0 \tag{2.12}$$

Chapter 3

Numerical Methods

3.1 CFD Turbulence models

There are different approaches to solve incompressible turbulent flow, which depends on required accuracy to capture the physics and the computational cost involved. Reynolds Averaged Navies Stokes (RANS) solves time averaged quantity and thus provide reasonably good results with less computational cost involved. Large-Eddy Simulation (LES) models the small scale eddies and resolves the large scale eddies and thus requires finer mesh in order to capture smaller eddies, which gives better accuracy compared to RANS approach but computational cost increases due to finer mesh. Hybrid RANS/LES takes the advantage of both the approaches, by using RANS approach near to the region of smaller eddies formation and LES approach for the larger eddies. Computational cost is reduces by having coarser mesh near to capture smaller eddies and accuracy is comparatively higher than the RANS approach. RANS and LES approach formulation is needed in order to understand Hybrid RANS/LES approach.

3.1.1 Reynolds Averaged Navier Stokes(RANS)

It is not necessary that all physical length scales be resolved for engineering applications, as the area of interest are only the mean properties of the flow.The computational time required for a DNS calculation is significantly less so it has been developed, Reynolds Averaged Navies Stokes (RANS) equations contain the instantaneous governing equations which are averaged in time. The turbulent Reynolds stress term, $\rho(\overline{u_i' u_j'})$ in the momentum equation is often modelled using the concept proposed by Boussinesq, where the turbulent stresses are proportional to gradients in mean velocity:

$$rho(\overline{u_i' u_j'}) = 2\mu_t \left(\overline{S}_{ij} - \frac{1}{3} \frac{\partial \overline{U}_k}{\partial x_k} \delta_{ij} \right) \tag{3.1}$$

$$k = \frac{1}{2}\overline{u_i' u_j'} \tag{3.2}$$

Where μ_t is turbulent viscosity and k is mean turbulent energy per unit mass.

3.1.2 Large Eddy Simulation(LES)

LES deals with direct capturing of highly energetic large scale eddy and models the more universal small scale eddies through different sub-scale models. Smaller eddies have an important role in providing the physical meaning, giving overall dissipation to the large scale structures, and this is modelled by LES approach. LES aims to improve accuracy obtained by RANS approach. LES shows up with better capturing of turbulence structure by direct resolution of large scale eddies where as in Direct Numerical Simulation (DNS) complete flow domain is directly resolved using full range of eddies without any modelling, as a result grid size and time step is depicted by small eddies of kolmogorov length scale which increase the total computational cost and making DNS currently not possible for high Reynold number flows. Capturing of flow over duct using LES approach gives a clearer picture of the turbulent nature of the wake , with a wide range of turbulent scales. OpenFoam offers number of model for μ_t calculations, namely Smagorinsky SGS model, KEqn model, Dynamic one equation eddy-viscosity model and WALE model. The equation for LES can be obtained by applying a filter to the instantaneous governing equations. A filtered variable is defined as:

$$\overline{\phi}(x) = \int_D \phi(x^*)G(x - x^*)dx^* \tag{3.3}$$

Where $G(x - x^*)$ is the filter function. The top-hat filter is a sharp cutoff filter, where the large enough eddies are captured, or smaller ones are modelled. To be able to capture the large scale eddies of turbulent flow in a given computational mesh domain, the filter width should be below the inertial range of the turbulence spectrum.

$$G(x) = \begin{cases} 1/\Delta, & x \leq \Delta/2 \\ 0, & \text{otherwise} \end{cases} \tag{3.4}$$

Where Δ is the filter width,

$$\Delta = max(\delta_x, \delta_y, \delta_z) \tag{3.5}$$

$\delta_x, \delta_y, \delta_z$ are the mesh cell size in x, y and z direction respectively.

- **Smagorinsky-Lilly model**

  The model developed by Smagorinsky is one of the widely used subgrid-scale in modelling the turbulent flows . The way in which turbulent viscosity is calculated is modified slightly compare to RANS and is referred to as the subgrid-scale (SGS) viscosity (μ_{SGS}). This subgrid viscosity is used for modelling the energy dissipation that the small (subgrid) scales give to the large scale turbulence.

$$\mu_{SGS} = \rho(C_s\Delta)^2|\tilde{S}| \tag{3.6}$$

$$|S| = \sqrt{2S_{ij}S_{ij}} \tag{3.7}$$

  $\overline{S}_{ij}$ is strain rate tensor where, C_s is a Smagorinsky constant whose value ranges from 0.1-0.2. This model was obtained based on the assumption that subgrid-scales are in equilibrium, meaning the production and destruction terms of energy equation are balanced.

3.1.3 Hybrid RANS / LES or Detached Eddy Simulation(DES) approach

The computational cost of fully resolved LES can be reduced by relaxing the requirements on mesh spacing by solving the full system of Reynolds averaged Navier Stokes equations for the near wall region, particularly in the parallel direction of the surface. Standard RANS turbulence models could still be used, using a transition to LES which occurs far away from the surface. Figure 3.1 shows a comparison between different approaches to turbulence modelling. In the RANS and LES regions we can identify a stronger coupling than what is identifiable in two layer approach, since all required fluxes are calculated across this boundary. However there can be a discontinuous eddy viscosity profile because of the transitioning from RANS to SGS turbulence models. However, the extent of this transitioning could be controlled by intelligent use of blending function between the two regions. Detached eddy simulation (DES) was developed by Spalart[34] and it paved way for a hybrid RANS-LES method which uses a single turbulence model for both the regions, namely
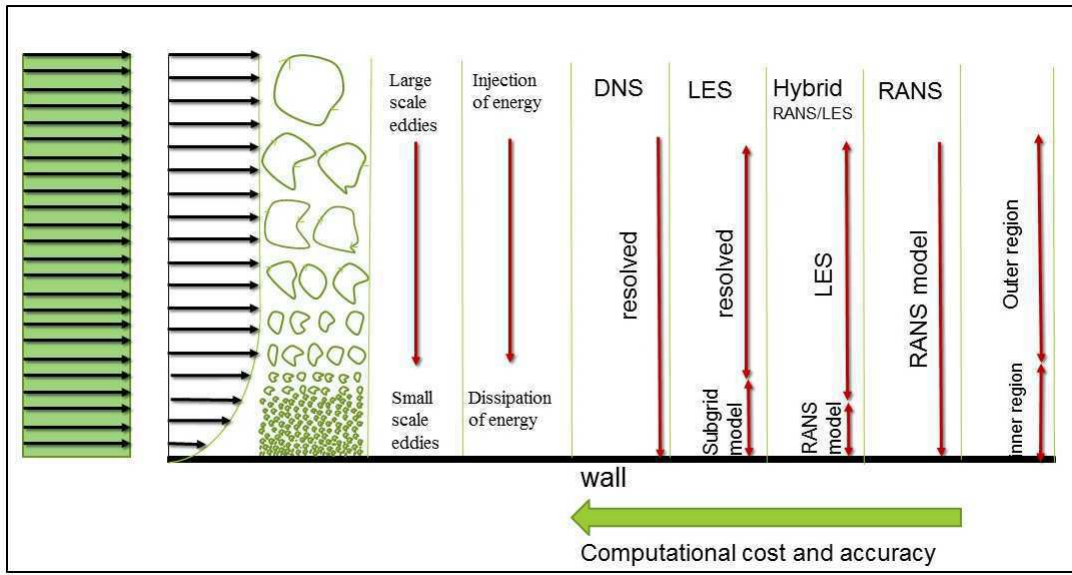

Figure 3.1: Comparison between DNS, RANS, LES and Hybrid RANS/ LES approach.[35]

the near wall RANS regions and the free-stream regions. DES was basically formulated with help of the Spalart-Allmaras turbulence model because of its robust nature and suitability for modelling boundary flows. It is easy to transform this turbulence model into that of a Smagorinsky type SGS model when the production and destruction terms in the transport equation are balanced for kinematic eddy viscosity equation 3.8, giving:

$$\frac{\partial \rho \tilde{\nu}}{\partial t} + \frac{\partial \rho u_i \tilde{\nu}}{\partial x_i} = D_{\tilde{\nu}} + P_{\tilde{\nu}}^+ + P_{\tilde{\nu}}^- \tag{3.8}$$

Whereare the terms $D_{\tilde{\nu}} + P_{\tilde{\nu}}^+ + P_{\tilde{\nu}}^-$ modeling diffusion, production and destruction

$$C_{b1}\tilde{s}\tilde{\nu} = c_{w1}\left(\frac{\tilde{\nu}}{d}\right)^2 \tag{3.9}$$

where, C_{b1} and c_{w1} are model constants and, critically, d is the RANS turbulence length scale which

is given by the distance to the nearest wall, y_w.

$$\mu_t = \rho \tilde{\nu} f_{\nu 1} \tag{3.10}$$

With some manipulation and using Equation 3.10 this becomes:

$$\mu_t = \rho \tilde{S} d^2 \tag{3.11}$$

it is straightforward to see that a Smagorinsky type model can be achieved through alteration of the turbulence length scale from d in the RANS region to $C_{DES}\Delta$ in the free-stream, where C_{DES} is a model constant. The transition between these length scales is made possible through the introduction of a new variable $\tilde{d}$ in place of d, in the kinematic eddy viscosity transport equation, defined as:

$$\tilde{d} = min(y_w, C_{DES}\Delta) \tag{3.12}$$

This assumes that the production and destruction terms are dominant in an equilibrium flow (i.e. the diffusion term is negligible) and so they can be equated to form the Smagorinsky like model. This new length scale acts as a sharp switching function between the RANS and LES approaches and is dependent upon mesh resolution and the method used to calculate the filter width. Special care needs to be taken when designing the grid on which a DES is to be conducted [36] in order to ensure transition to LES occurs outside of the boundary layer. The recommended filter width[37] is that given by 3.5. DES is not restricted to use with the Spalart-Allmaras turbulence model and Strelets formulated version which uses the Menter SST turbulence model, citing its good performance in boundary layer calculations and separation prediction as to why it would make an ideal candidate for RANS modelling in the near wall region. The RANS length scale is defined as:

$$l_{k-\omega} = \frac{k^{\frac{1}{2}}}{\beta^* \omega} \tag{3.13}$$

Again, it is required that for an equilibrium free-stream ow the k and ω transport equations are modified such that the turbulent viscosity of the Menter SST turbulence model reduces to a Smagorinsky like form. For simplicity, Strelets [46] suggested a modification to just the diffusion term in the k3.14 , from

$$\frac{\partial \rho k}{\partial t} + \frac{\partial \rho u_i k}{\partial x_i} = D_k + P_k^+ + P_k^- \tag{3.14}$$

$$D_k = \rho \beta^* k \omega = \frac{\rho k^{\frac{1}{2}}}{l_{k-\omega}} \tag{3.15}$$

To

$$D_{k,DES} = \frac{\rho k^{\frac{1}{2}}}{\tilde{l}} \tag{3.16}$$

where $\tilde{l}$ is is the DES turbulence length scale, given as:

$$\tilde{l} = min(l_{k-\omega}, C_{DES}\Delta) \tag{3.17}$$

Since the Menter SST turbulence model transitions between the $k - \omega$ and $k - \epsilon$ turbulence models using a blending function F_1, it is possible the sub-grid viscosity could be calculated using either

model, since the transition between models may not coincide with the transition to LES. For this reason, there exists a C_{DES} constant for each model, and that used in the calculation for $\tilde{l}$ must be found using the blending function:

$$C_{DES} = (1 - F_1)C_{DES}^{k-\omega} + F_1 C_{DES}^{k-\epsilon} \tag{3.18}$$

However, use of the $k - \epsilon$ model is more likely since the $k - \omega$ turbulence model is only active near the wall. These model constants were tuned by simulating the decay of homogeneous isotropic turbulence and were found to be $C_{DES}^{k-\omega} = 0.61$ and $C_{DES}^{k-\epsilon} = 0.78$. For DES with the Spalart-Allmaras turbulence model C_{DES} was tuned to a value of 0.65.

3.2   OpenFOAM

OpenFOAM stands for "Open-source Field Operation And Manipulation". The governing equations are solved using the Open Foam solvers. Open foam contains the different CFD solvers to solve the fluid flow equations. Brief details of open foam are given below and more details can be found in the reference [38] .It is used widely in academia and industry to solve wide variety of computational problems. In contrast to other proprietary software, the source code here is accessible and modifiable.

The OpenFOAM utilities are subdivided into:

- **Mesh conversion:**
  Utilities to convert mesh generated from third partymeshing tools like Ansys, GMSH,etc. to OpenFOAM format

- **Parallel Processing units:**
  Tools to decompose, reconstruct and redistributethe computational case to perform parallel calculations, at times better than other CFD software.

- **Post-Processing units:**
  Data can be visualized using paraview, can be exported to other softwarefor visualizationsuch as Ensight, Mayavi

There are many solvers available in OpenFOAM focussing on laminar and tubulence flows incompressible and compressible fluids, multiphase flows, LES and DNS turbulence models, etc. The present problem concentrates on incompressible turbulence flows.

In OpenFOAM a certain structure of the input files is expected. A case has to be set up in a predestined manner which contains a minimum of three directories. A constant folder and a system folder are needed. Also a time folder is needed, this is usually named 0, but can be named differently if 0 is not the starting time. There are also subfolders and files that are contained in the mentioned folders, a few options are reviewed here.

3.2.1   0 Folder

This folder contains files with the initial conditions of the used variables. For laminar incompressible Navier Stokes equation only files containing initial conditions of p and U are needed. For turbulence models or compressible flow other variables will need to be added as well. Three entries have to be done for each variable file. The dimension of the variable is assigned through dimensions in the file (for instance m/s for the velocity). The internal field is assigned through internalField and the boundary field is given through boundaryField

3.2.2   Constant Folder

This folder contains specifications for turbulence and fluid properties. Depending on the solver chosen, different files need to be specified. For all solvers which calculate the RANS equations, the file RASProperties determines the turbulence model used. The type of turbulence model applied is determined in turbulenceProperties where either LES, RAS or laminar model can be chosen. For incompressible solvers the file transportProperties determines the behaviour of the kinematic viscosity.

It also has another folder named **PolyMesh** where files which describe the mesh are there. These files include points, which contain the points of the mesh faces, which contain the faces of the cells. owner, that contains what faces belong to a cell and neighbour which contains the information about the connectivity between cells. Also the boundaries are given in the file boundary, here the boundaries are assigned names and also of what type they are, such as empty, wall or patch for instance. eg.

Table 3.1: Type of boundaries used in openfoam.

Location	Type of Boundary condition
Inlet	Patch(flow from inlet)
top	Wall
bottom	Wall
wall1	Wall
wall2	Wall
outlet	Patch(flow through outlet)

3.2.3   system Folder

This folder contains several files where the specifications for the simulation are mentioned

- **decomposeParDict file:**

  The mesh is decomposed into an assigned number of parts for parallel simulations.

- **controlDict file:**

  The frequency of solution file outputs, run time, time steps and Courant number are assigned. Few keywords used here are

  1. **startFrom-** Controls the start time of the simulation.

     – **firstTime:** Earliest time step from the set of time directories.

     – **startTime:** Time specified by the startTime keyword entry.

     – **latestTime:** Most recent time step from the set of time directories.

  2. **stopAt-** Controls the end time of the simulation.

     – **endTime:** Time specified by the endTime keyword entry.

     – **writeNow:** Stops simulation on completion of current time step and writes data

     – **noWriteNow:** Stops simulation on completion of current time step and does not write out data.

     – **nextWrite:** Stops simulation on completion of next scheduled write time, specified by writeControl.

  3. **endTime-** End time for the simulation when stopAt endTime; is specified.

  4. **deltaT-** Time step of the simulation.

- **fvSchemes:**

  In the fvSchemes file the numerical discretization schemes for the different components in the modelled equations are assigned. For time discretization the schemes shown in table 3.2 are available . They are assigned under ddtSchemes in the fvSchemes file. In the CrankNicholson case a blending function parameter $\psi\epsilon[0,1]$ can be chosen. For $\psi = 1$, the normal Crank-Nicholson scheme is used,

Table 3.2: Time Schemes.

Euler	First order, bounded, implicit
localEuler	Local-time step, first order, bounded, implicit
CrankNicholson ψ	Second order, bounded, implicit
backward	Second order, implicit
steadyState	No solving of time derivatives

The **gradSchemes** sub-dictionary contains gradient terms. The default discretisation scheme that is primarily used for gradient terms is default Gauss linear; The Gauss entry specifies the

standard finite volume discretisation of Gaussian integration which requires the interpolation of values from cell centres to face centres.

The **divSchemes** sub-dictionary contains divergence terms, i.e. terms of the form $\nabla\cdot$, excluding Laplacian terms (of the form $\nabla \cdot (\Gamma\nabla...)$). This includes both advection terms, where velocity U provides the advective flux, and other terms, that are often diffusive in nature.

The **snGradSchemes** sub-dictionary contains surface normal gradient terms. The various schemes are presented in table 3.3

Table 3.3: Surface normal gradients for laplacian terms calculations.

corrected	Explicit non-orthogonal correction
uncorrected	No non-orthogonal correction
limited	Limited non-orthogonal correction implicit
bounded	Bounded correction
fourth	Fourth order

- **fvSolution:**

In this file the linear solvers for the sequential equations are assigned. Also the linear solver tolerance and maximum number of iterations are assigned here. In OpenFOAM the available linear solvers are preconditioned conjugate or bi-conjugate gradient solvers, smooth solvers, generalized geometric algebraic multi-grid (GAMG) solvers and also diagonal solvers (for explicit systems). The conjugate gradient solvers can use the preconditioners diagonal-incomplete LU (DILU for asymmetric systems), diagonal-incomplete Cholesky (DIC for symmetric systems), diagonal preconditioning and GAMG preconditioning. Available smoothers are Gauss-Seidel and Diagonal incomplete-Cholesky (for symmetric matrices). Under relaxation of the sequential equations can be set in this file, and if SIMPLE or PISO algorithms are used settings for these can also be specified.

3.3   Solution Methodology

Governing equations are discretized and solved using Finite Volume methods with a incompressible turbulence based solver. In the current work buoyantBoussinesqPimpleFoam solver has been used with transient time stepping for all the simulations. The solver setting is shown in below table 3.4

Table 3.4: OpenFOAM solver settings

Solver	buoyantBoussinesqPimpleFoam
Time	Transient
Models	kOmegaSSTDES, SpalartAllmarasDES
Material	Air
Spatial discretization for ow	Second order upwind
Flux type	Kurganov-Tadmor
Transient formulation	First order upwind
Courant number	Adjustable

3.4 Mesh details

For all the Meshes, geometry is generated in Ansys ICEM CFD and after the geometric model is generated then planer 2D blocking is done. By blocking strategy to produce structured meshing, geometry is split into number of rectangular blocks in such away that whole geometry is covered. Then association of edges and vertices is performed and number of nodes on each edges is given as per required mesh and then mesh generation is performed to obtain desired mesh.

1. **Turbulent flow over single square cylinder.**

   To know the solver capability with respect to capturing the exact heat transfer coefficient of turbulent flow over an object. We have solved a benchmark problem of flow over a single square cylinder. Flow over square cylinder is implicated in many devices to study the flow separation zone, wake region and vortex formation downstream of the cylinder. The simulation is carried out by Hybrid RANS/LES approach consisting komegaSST and spalartAllmaras. The simulated results are validated against experimental data. Computational domain and meshing is shown in 3.2. Geometric and flow parameters of the flow over single square cylinder are: Cylinder side h = D, domain height H = 20D, domain length L = $40D$. Reynolds number $Re = 22000$, inlet temperature is$293K$ and temperature of square walls are kept constant at $320K$. Grid size is kept constant for both the solvers at 46400. Mesh domain of single square cylinder
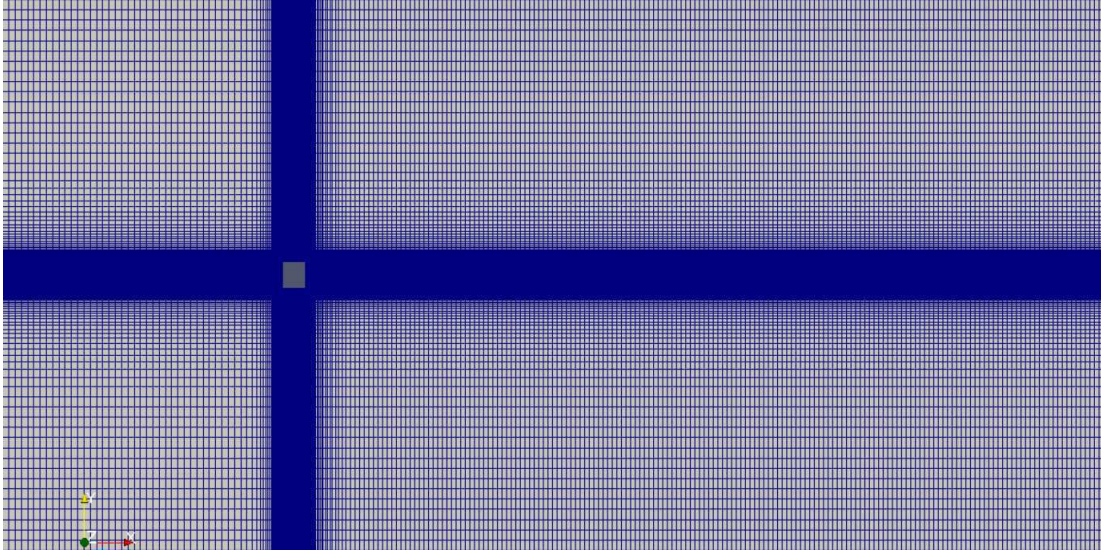
Figure 3.2: Mesh domain of single square cylinder

2. **Turbulent flow over tandem square cylinders**

   The results provided in the next chapter are obtained using kOmegaSSTDES for flow over tandem square cylinders for a different Reynolds number, spacings and sizes of the cylinders. Geometric and flow parameters of the square cylinders are: Cylinder side h = D, domain height $H = 15D$, domain length $L = 32.5D$. Inlet temperature is $300K$ and temperature of square walls are kept constant at 330 K. Grid independence test were done for three grids and the grid size of 75000 is used to obtain all the results is shown in 3.3
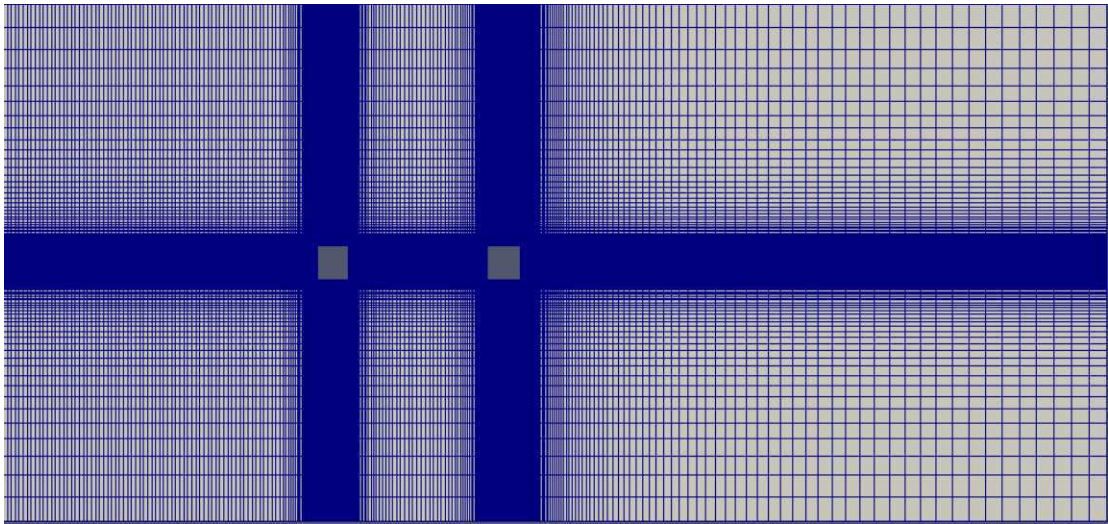
Figure 3.3: Mesh domain of tandem square cylinder

Chapter 4

Results

The accuracy of numerical method of Hybrid RANS/LES is analyzed by taking a benchmark problem of single square cylinder and comparing the different Hybrid approaches with the available experimental results is shown. Second validation involving tandem cylinders are also done to check the accuracy for tandem cylinders. Study of tandem square cylinders for different Reynolds number, spacings, sizes and configurations of cylinders are done and the following results are shown.

4.1   Validation of turbulent ow over single square cylinder

The flow over single cylinder is considered most widely used separated ow geometry for validation and study of the wake dynamics. The wake of a backward-facing step has unique features mainly in two regions: in near wake and far wake regions. Due to instabilities, the vortices in the shear layer roll up and pair with the adjacent vortices to form larger coherent structure. The accuracy of present numerical methods is conrmed by validating current results with the experimental results available in the literature. Inlet ow eld characteristics are of Reynolds number of 22000, free stream temperature $T_0 = 293K$ and cylinder walls are considered as constant wall temperature boundary condition. Contour plots of vorticity, velocity and temperature is shown in 4.1, 4.2 and4.3 According
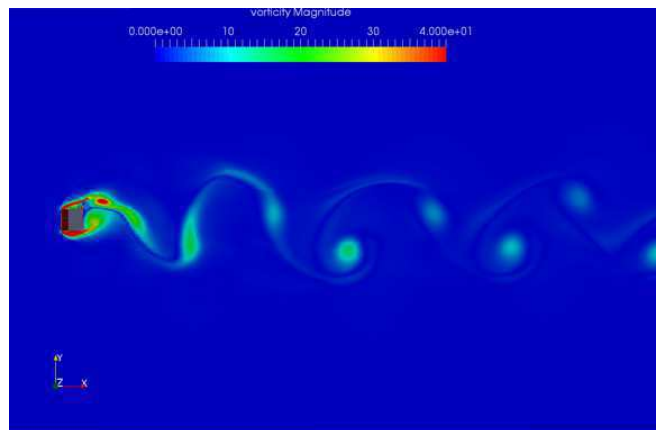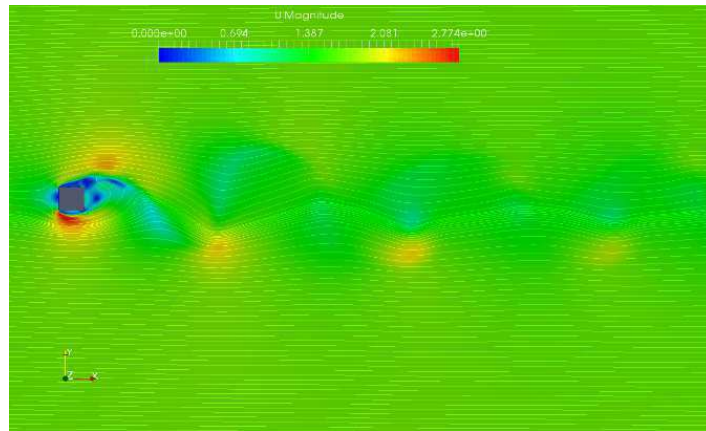

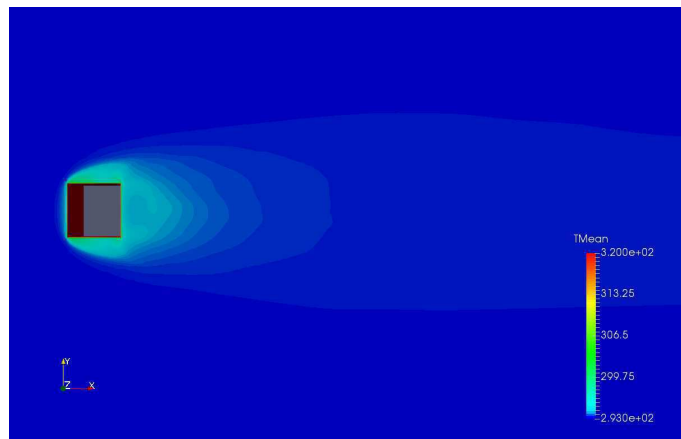Figure 4.1: vorticity contour

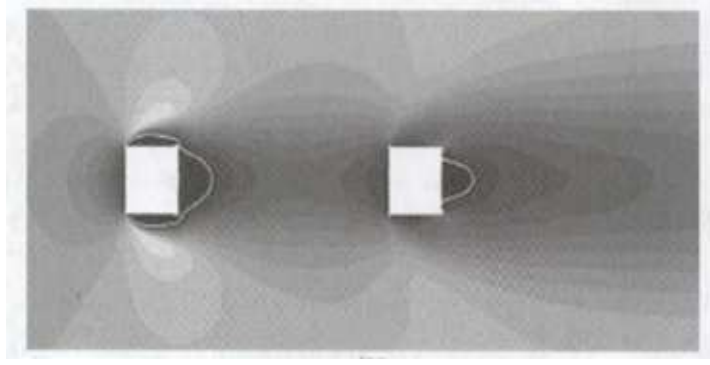Figure 4.2: velocity contour

Figure 4.3: Temperature contour

Figure 4.4: Isocontours of streamwise time averaged velocity taken form Duchaine[32] for comparison

to the results the numerial Mean Nusselt number by using komegaSSTDES model was found to be 196.5 and by using spalartAllmarasDES model was found to be 190. The obtained results were compared with the Gnielinski correlation[39] obtained experimentally,

$$Nu = 0.3 + \sqrt{Nu_l^2 + Nu_t^2} \qquad (4.1)$$

where,

$$Nu_l = 0.664 Pr^{\frac{1}{3}} Re_{2d}^{\frac{1}{2}} \qquad (4.2)$$

and

$$Nu_t = \frac{0.037 Pr Re_{2d}^{0.8}}{1 - 2.443 Re_{2d}^{-0.1}(Pr^{2/3} - 1)} \qquad (4.3)$$

According to the Gnielinski correlation the average Nusselt number for flow is found to be 200. Error obtained by komegaSSTDES model(2% error) is about 3 % less than the error in SplaratAllmaras-DES model(5% error) when compared with Gnielinski correlation. It is concluded that komegaSST-DES solver is more accurate result compared to SpalartAllmaras solver. It is decided to use kOmegaSSTDES model for getting results with flow over tandem cylinder configuration.

4.2 Validation and grid independence for flow over tandem square cylinders

A Detched Eddy Simulation study has been conducted for a ow past a heated tandem square cylinder with three computational grids for $Re = 16,000$. The both grids have been designed to be manageable on typical workstation level. The DES ow results have been compared with experimental data. The accuracy of the present DES technique has been demonstrated. In general, the Detached Eddy Simulation results are comparable with regard to the global quantities and ow behaviour and the calculated average total heat transfer is nearly the same as for all grids. The results are shown in figure 4.5 and 4.4

Axial velocity profiles in the neighbouring of the cylinders: A comparison between mean axial velocity on the upper face of each cylinder with the experimental data of Reference [16] for an isolated cylinder. The numerical results concerning the upstream cylinder agree with the experimental profiles. For the first obstacle, the velocity levels match the experimental results. Nevertheless, the
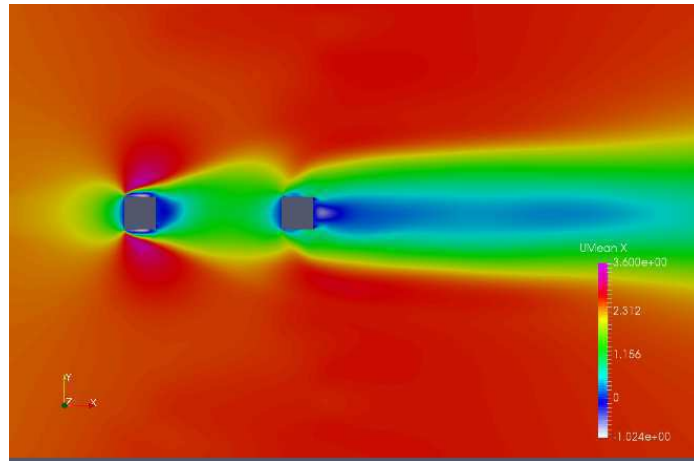
Figure 4.5: Isocontours of streamwise time averaged velocity

velocity of the recirculating flow is lower and a slight shift is observed in the position of the shear zone located far away from the wall in the computation. Due to the wake of the upstream cylinder, the velocity profiles of the downstream cylinder exhibit a deficit of velocity. The velocity gradients are smaller for the second cylinder. As shown in figure 4.6,4.7,4.8 and 4.9, axial velocity profiles show that there is no recirculation zone on lateral faces of the downstream cylinder. The inflection of the last two profiles ($x/D = 0.75$ and $x/D = 1.0$) is due to upstream propagation of vortices coming from the downstream face.
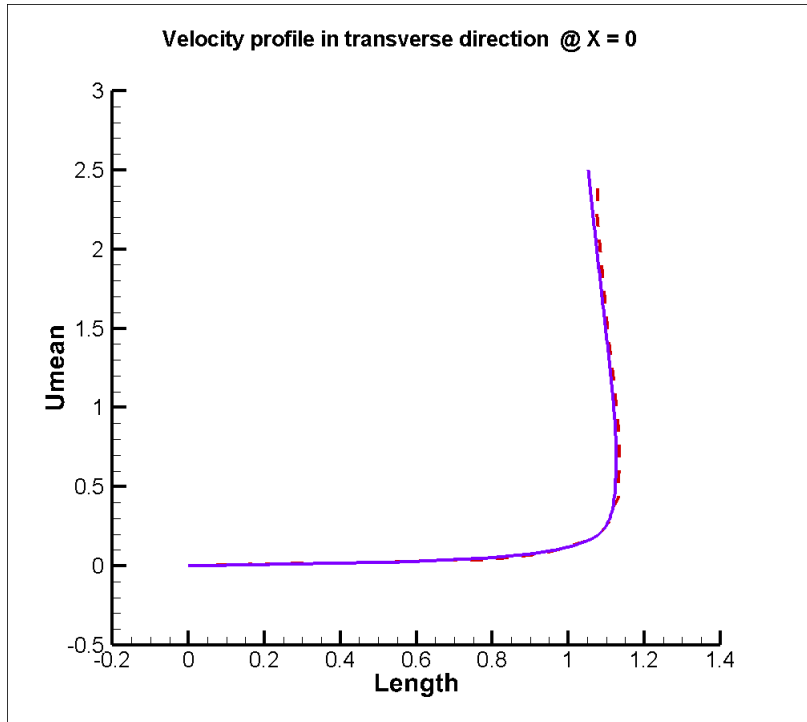
Figure 4.6: Plot comparison of velocity at different points across top surface with experimental results at x/D = 0
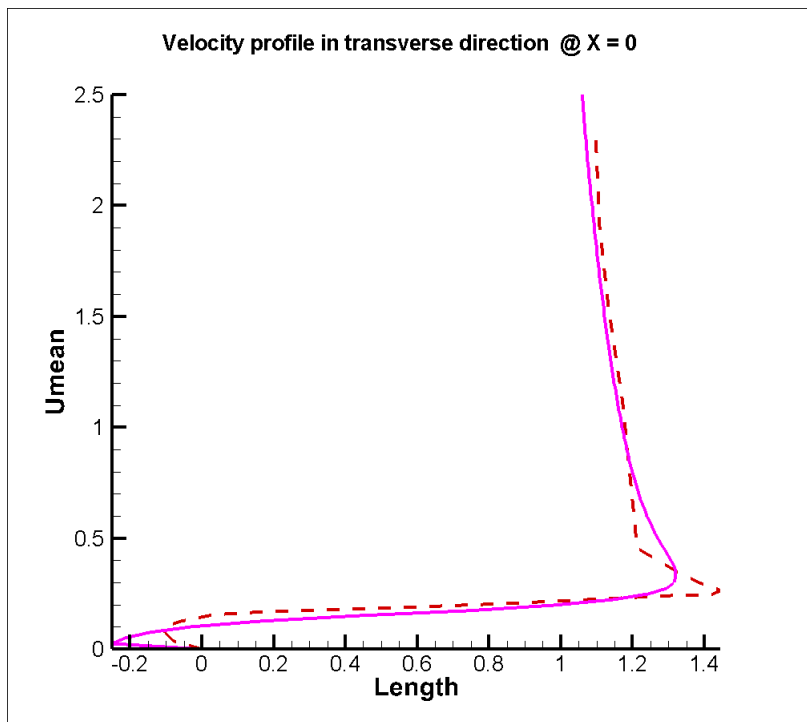

Figure 4.7: Plot comparison of velocity at different points across top surface with experimental results at x/D = 0.25
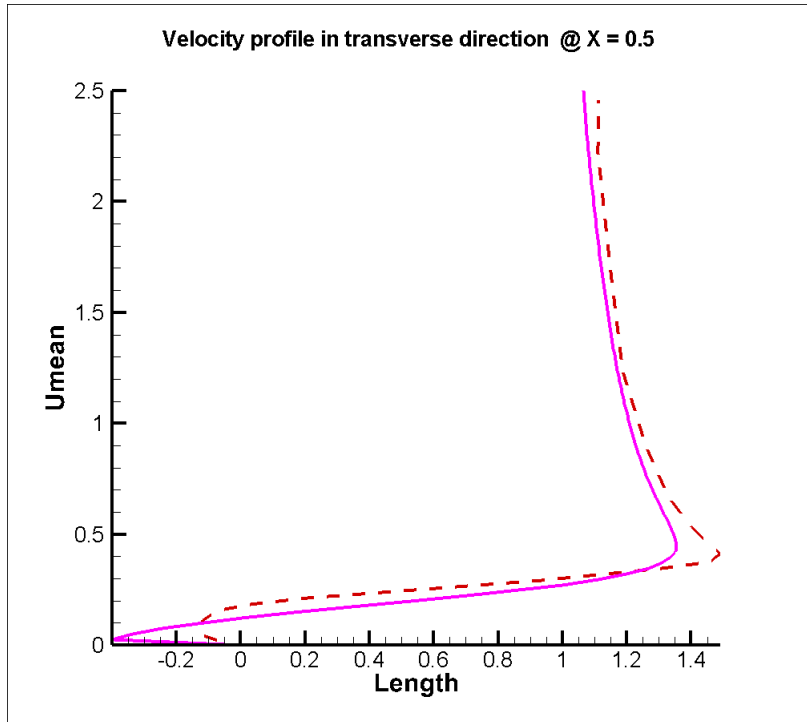
Figure 4.8: Plot comparison of velocity at different points across top surface with experimental results at x/D = 0.75
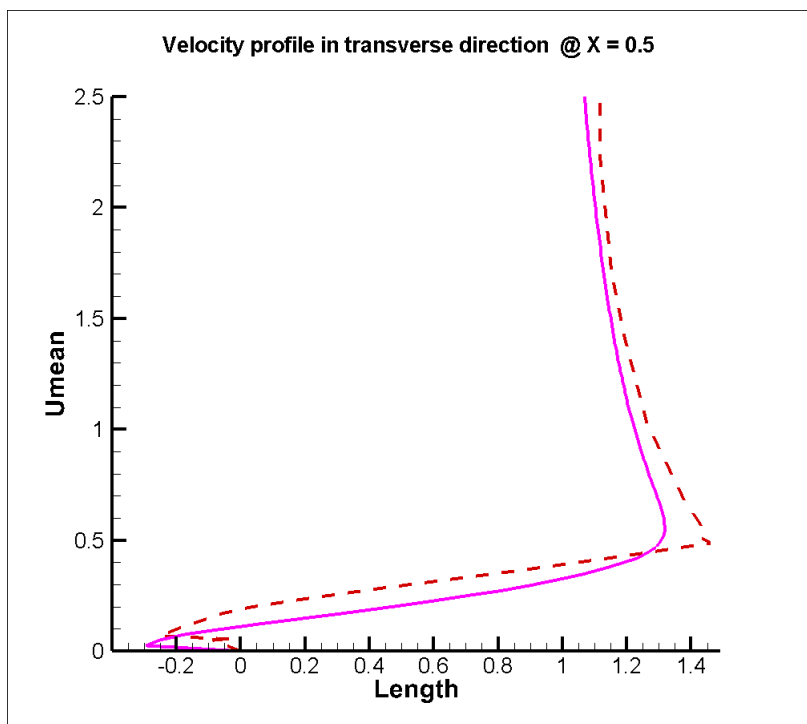

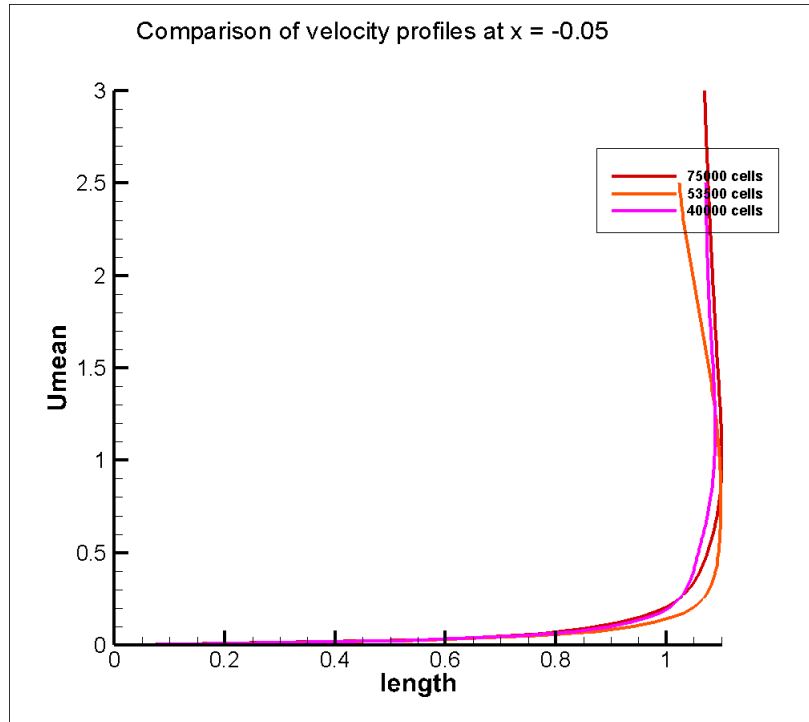Figure 4.9: Plot comparison of velocity at different points across top surface with experimental results at x/D = 1

Figure 4.10: A comparison between mean axial velocity on the upper face of cylinder is plotted for different meshes at x/D = 0

4.2.1 Grid independence

Grid convergence test is carried out by simulating three dierent mesh sizes for Reynolds number $Re = 16000$ and $T_w = 330K$. A comparison between mean axial velocity on the upper face of each cylinder is plotted as shown in gure 4.10,4.11,4.12,4.13 and 4.14 with dierent mesh sizes of coarse mesh 40000, medium mesh 53000 and ne mesh 75000 cells and also average Nusselt number of both upstream and downstream cylinders are given in table 4.1 and 4.2. It can be seen that solution is grid independent and performance parameter chosen is having very less variation for medium and ne mesh. Hence fine grid (Grid 1) is chosen for all the simulations reported.

Table 4.1: Average Nusselt number of 4 sides of upstream square cylinder with different meshes

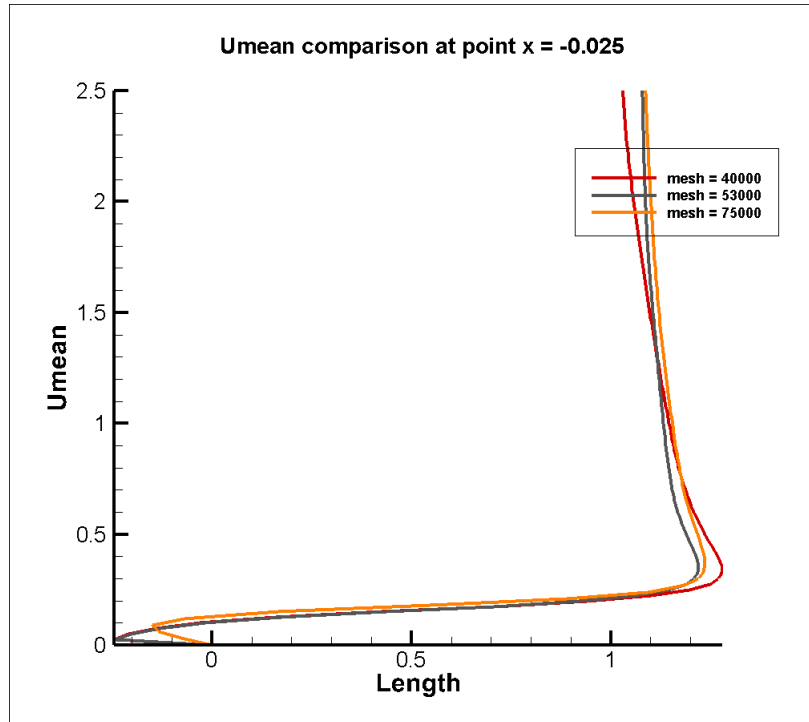|	Nusselt number 75000 cells	Nusselt number 53500 cells	Nusselt number 40000 cells
Front	115.4367	114.9611	113.7167
Bottom	80.1267	78.3294	76.195
Top	79.0767	78.5817	76.3183
rear	76.47	76.4933	79.3583
Overall average	87.7725	87.09135	86.3971

Figure 4.11: A comparison between mean axial velocity on the upper face of cylinder is plotted for different meshes at x/D = 0.25

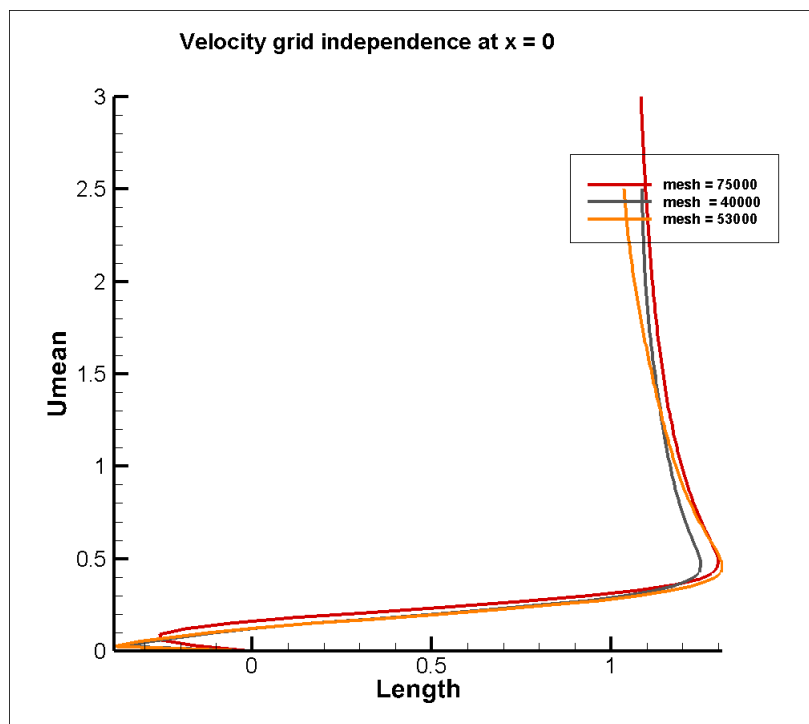Figure 4.12: A comparison between mean axial velocity on the upper face of cylinder is plotted for different meshes at x/D = 0.5
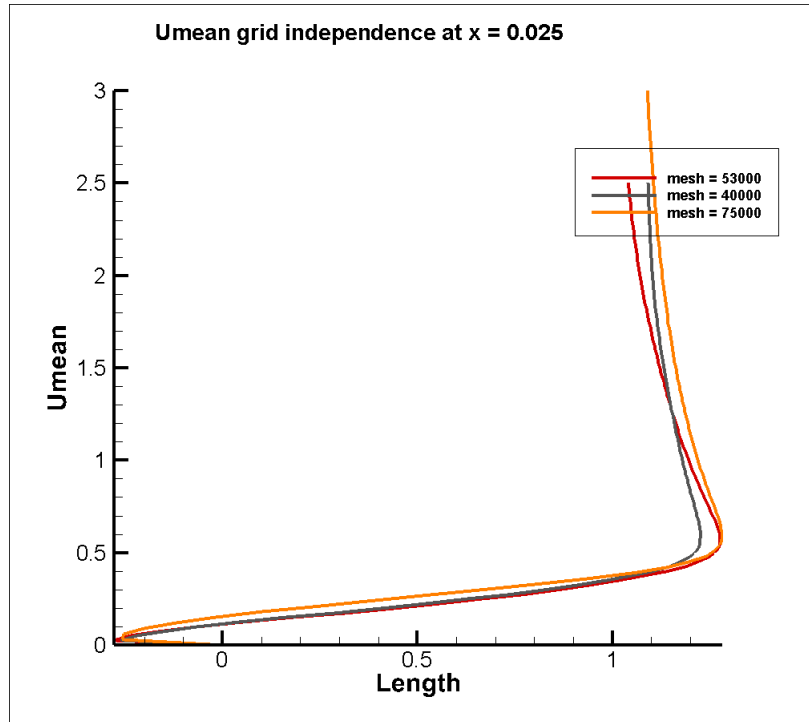
Figure 4.13: A comparison between mean axial velocity on the upper face of cylinder is plotted for different meshes at x/D = 0.75

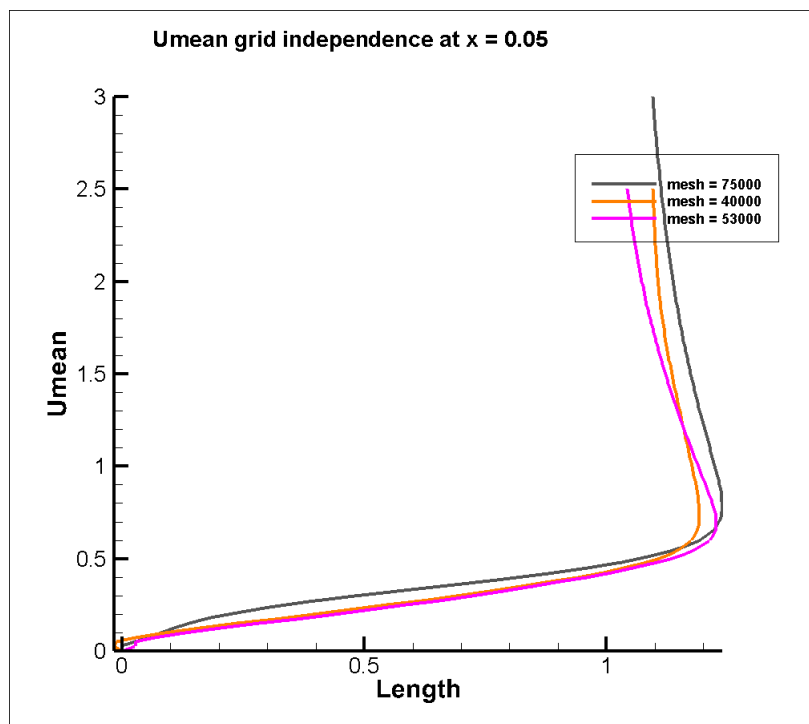
Figure 4.14: A comparison between mean axial velocity on the upper face of cylinder is plotted for different meshes at x/D = 1

Table 4.2: Average Nusselt number of 4 sides of downstream square cylinder with different meshes

	Nusselt number 75000 cells	Nusselt number 53500 cells	Nusselt number 40000 cells
Front	106.5867	105.9272	103.69
Bottom	89.8433	88.2172	86.08
Top	89.6933	88.1583	85.7
rear	87.76	85.2817	84.0467
Overall average	93.47085	91.8961	89.87

4.3 Effect of Reynolds number, spacings and sizes on heat transfer

The average Nusselt number increases with increasing Reynolds number as shown in table 4.3 . The results are carried out for 4 Reynolds number $16000, 28000, 32000$ and 40000. We can observe from the given values that effect of Reynolds number on upstream cylinder is more than that of downstream cylinder as the increase in Nusselt number is higher in case of upstream cylinder than the downstream cylinder. This is due to the blockage of the flow before the downstream cylinder(due to the upstream cylinder.)

Table 4.3: Average Nusselt number for 4 different Reynolds number

Reynolds Number	16000	28000	32000	40000
Upstream cylinder	87.77	99.528	103.148	110.95
Downstream cylinder	93.47	99.09	102.68	108.29

The simulations are done by increasing the spacing from $2D$ to $5D$ at Reynolds number of 16000. We can observe three kinds of regime that develops with different spacings. In Regime I ($s = 2D$) is featured by alternating reattachment of the upstream-cylinder shear layers onto the downstream cylinder, quasi-steady vortex in the gap and alternate shedding from the downstream cylinder. The wake width and formation length are smallest and largest as the shear layer reattachment dampens the wake unsteadiness. The heat transfer is lower in the downstream cylinder in this regime because of reduced velocity due to blockage and the absence of the vortex shedding that is responsible for inducing higher heat transfer. In regime II, we can observe the bi-stable nature of the flow which leads to higher heat transfer due to formation of vortex shedding. In Regime III compared to those for the other regimes, the wake width and formation length are large and small, respectively, as the impingement/interaction of the upstream-cylinder-generated vortices with the downstream cylinder diverges the downstream-cylinder shear layers outward. The Nusselt number is higher in this regime as shown in table 4.4

Table 4.4: Average Nusselt number at different spacings

Spacing	2D	3D	4D	5D
Upstream cylinder	71.96	76.06	87.77	70.147
Downstream cylinder	72.63	76.73	93.47	67.9

The vorticity contours obtained verifies the presence of the 3 regimes are given below. The heat transfer increases with size of the cylinder for both the cylinders. The simulations by keeping one of the cylinder has a side of $1D$and other cylinder having a side $1.5D$ at the Reynolds number of
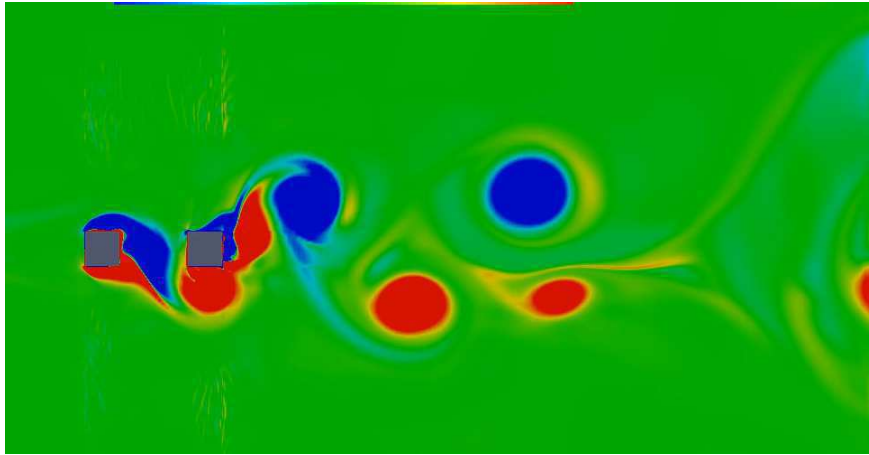
Figure 4.15: vorticity Contours at spacing of 2D
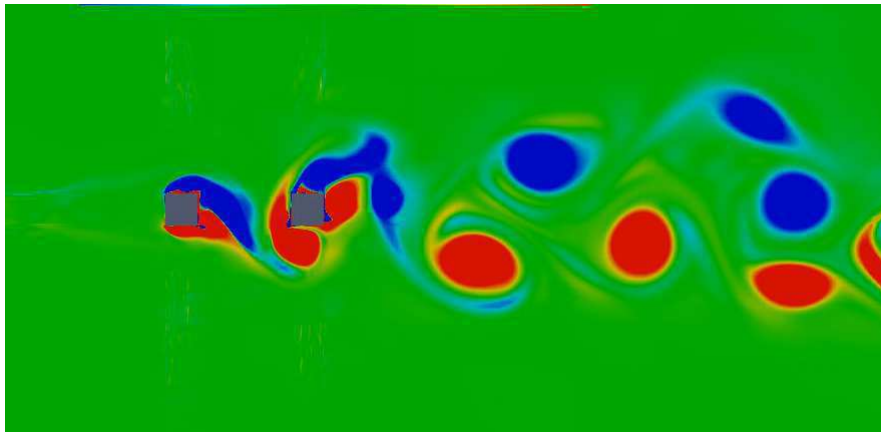

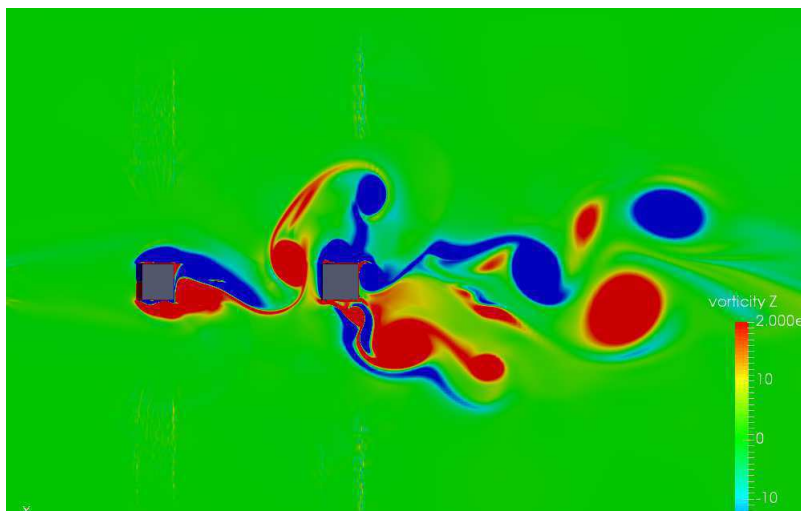Figure 4.16: vorticity Contours at spacing of 3D

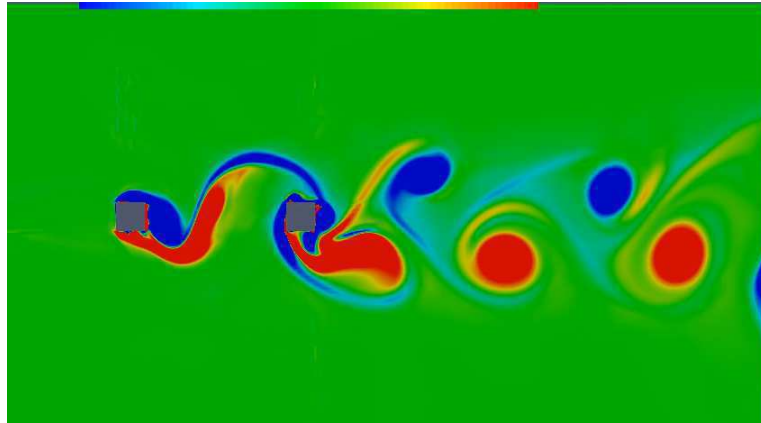Figure 4.17: vorticity Contours at spacing of 4D

Figure 4.18: vorticity Contours at spacing of 5D
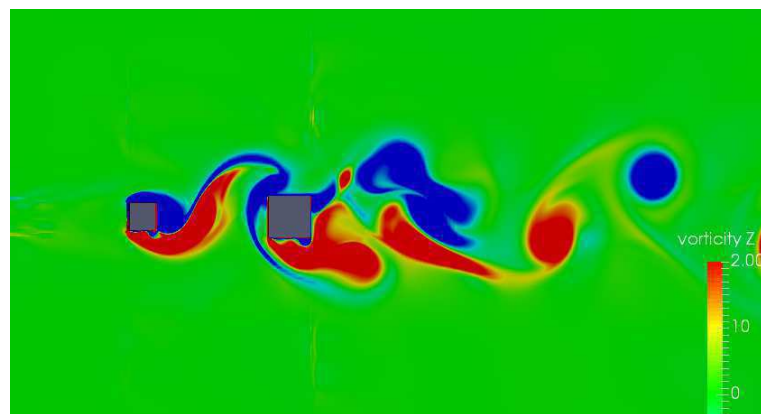
Figure 4.19: Vorticity contours of flow over square cylinder with bigger downstream cylinder

16000. The contours and values of average Nusselt number is shown in fig. 4.19, 4.20 and table 4.5. The Nusselt number for the cylinder with larger sides are higher for both downstream and upstream cylinders.

Table 4.5: Nusselt number values for different sizes of cylinder

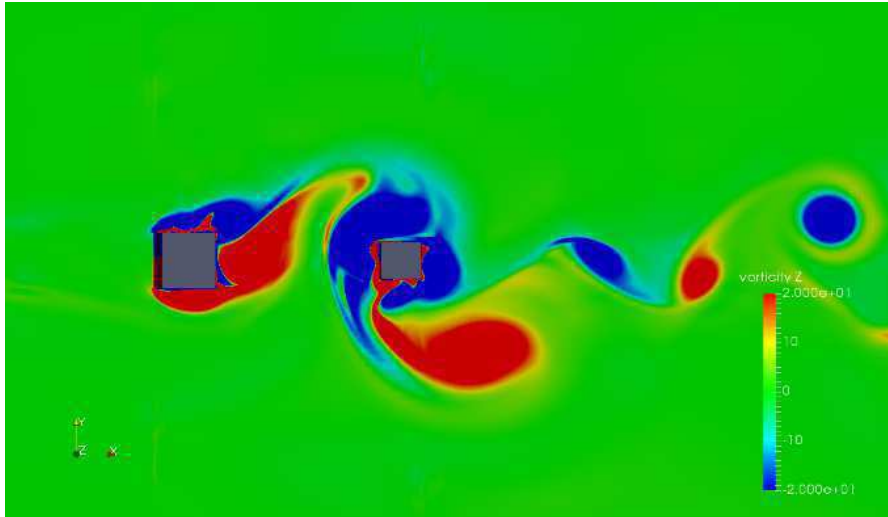|	Front bigger	Back bigger
Upstream cylinder	103.52	80.227
Downstream cylinder	72.305	95.737

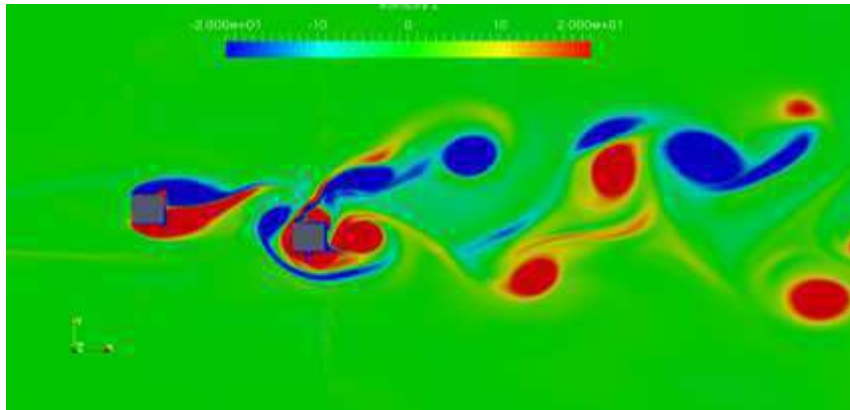Figure 4.20: Vorticity contours of flow over square cylinder with bigger upstream cylinder

Figure 4.21: Vorticity contours of flow over square cylinder when downstream cylinder is moved downwards by 1D

The heat transfer decreases when cylinders are in staggered configuration. The simulations ared done by moving downstream cylinder by a distance of $1D$ longitudinally with respect to the other cylinder upwards and downwards at a Reynolds number of 16000. The contours and values of average Nusselt number is shown in fig. 4.21, 4.22 and table 4.6. The Nusselt number for the cylinders in staggered configuration is lower for both downstream and upstream cylinders when compared with inline configuration.

Table 4.6: Nusselt number values for different sizes of cylinder

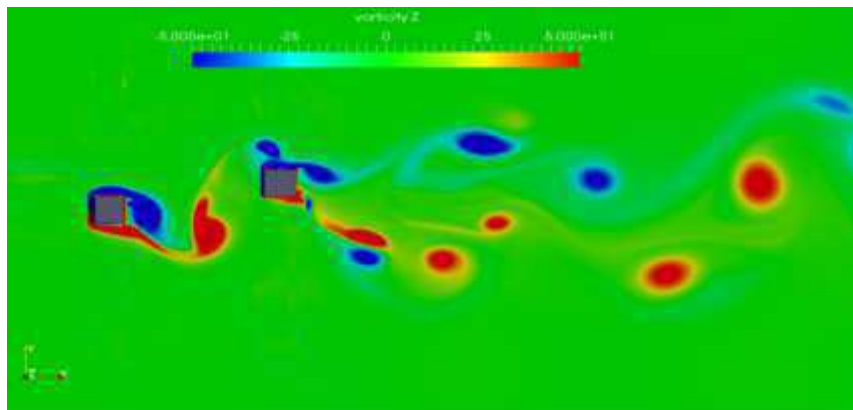|	Downstream cylinder moved downwards	Downstream cylinder moved ipwards
Upstream cylinder	60.623	74.553
Downstream cylinder	55.53	74.78

Figure 4.22: Vorticity contours of flow over square cylinder when downstream cylinder is moved upwards by 1D

Chapter 5

Conclusions

This work presents a DES of flow and heat transfer in a tandem configuration of two square cylinders at moderate Reynolds numbers by varying the Reynolds number ,spacings, sizes and configurations . DES on structured mesh is used to predict the flow structure and the heat transfer at the wall.The results are validated with experimental measurements performed on isolated cylinders. As far as aerodynamics and heat transfer are concerned, it is shown that the upstream cylinder behaves almost like an isolated cylinder. On the other hand, the wake of this first cylinder has an important impact on the second one. The analysis of the flow highlights two conflicting effects of the wake that play an important role in the heat load of the downstream obstacle: (i) A reduction of the mean velocity seen by the cylinder which reduces the Nusselt number, (ii)) The formation of vortex shedding. The Nusselt number for tandem square cylinder is 87.9(at Re=16000,s=4D) which has been found to be higher than that found at other spacing($Nu < 80$) and configurations(Nu 75). This shows that heat transfer is higher when the distance between the cylinder is around the critical spacing. The average Nusselt number increases with increasing Reynolds number due to increased mean velocity, decreases with decreasing spacings due to reduction in space for formation of vortex shedding and increases with increasing size The average Nusselt number for both the cylinders in tandem configuration is higher than that of staggered configuration.

References

[1] H. Schlichting. K. G, K Gersten, Boundary-layer theory 8 Ed 2000.

[2] B. Motameni. Two Circular Cylinders in Turbulent Cross Flow .

[3] A. Roshko. On the development of turbulent wakes from vortex streets .

[4] G. E. Karniadakis and G. S. Triantafyllou. Three-dimensional dynamics and transition to turbulence in the wake of bluff objects. *Journal of fluid mechanics* 238, (1992) 1–30.

[5] P. Bearman. On vortex shedding from a circular cylinder in the critical Reynolds number regime. *Journal of Fluid Mechanics* 37, (1969) 577–585.

[6] A. Roshko. Experiments on the flow past a circular cylinder at very high Reynolds number. *Journal of Fluid Mechanics* 10, (1961) 345–356.

[7] T. Igarashi. Characteristics of the flow around two circular cylinders arranged in tandem: 1st report. *Bulletin of JSME* 24, (1981) 323–331.

[8] D. Sumner. Two circular cylinders in cross-flow: a review. *Journal of Fluids and Structures* 26, (2010) 849–899.

[9] M. M. Alam, Y. Zhou, and X. Wang. The wake of two side-by-side square cylinders. *Journal of Fluid Mechanics* 669, (2011) 432–471.

[10] M. M. Alam, H. Bai, and Y. Zhou. The wake of two staggered square cylinders. *Journal of Fluid Mechanics* 801, (2016) 475–507.

[11] M. M. Alam, H. Sakamoto, and Y. Zhou. Determination of flow configurations and fluid forces acting on two staggered circular cylinders of equal diameter in cross-flow. *Journal of Fluids and Structures* 21, (2005) 363–394.

[12] J. Robichaux, S. Balachandar, and S. P. Vanka. Three-dimensional Floquet instability of the wake of square cylinder. *Physics of Fluids* 11, (1999) 560–578.

[13] D.-H. Yoon, K.-S. Yang, and C.-B. Choi. Flow past a square cylinder with an angle of incidence. *Physics of fluids* 22, (2010) 043,603.

[14] S. Luo, Y. Chew, and Y. Ng. Characteristics of square cylinder wake transition flows. *Physics of Fluids* 15, (2003) 2549–2559.

[15] S. Luo, X. Tong, and B. Khoo. Transition phenomena in the wake of a square cylinder. *Journal of Fluids and Structures* 23, (2007) 227–248.

[16] D. Lyn and W. Rodi. The flapping shear layer formed by flow separation from the forward corner of a square cylinder. *Journal of fluid Mechanics* 267, (1994) 353–376.

[17] C. Brun, S. Aubrun, T. Goossens, and P. Ravier. Coherent structures and their frequency signature in the separated shear layer on the sides of a square cylinder. *Flow, Turbulence and Combustion* 81, (2008) 97–114.

[18] M. Minguez, C. Brun, R. Pasquetti, and E. Serre. Experimental and high-order LES analysis of the flow in near-wall region of a square cylinder. *International Journal of Heat and Fluid Flow* 32, (2011) 558–566.

[19] Y. Cao and T. Tamura. Large-eddy simulations of flow past a square cylinder using structured and unstructured grids. *Computers & Fluids* 137, (2016) 36–54.

[20] T. Igarashi. Heat transfer from a square prism to an air stream. *International journal of heat and mass transfer* 28, (1985) 175–181.

[21] T. Igarashi. Local heat transfer from a square prism to an airstream. *International Journal of Heat and Mass Transfer* 29, (1986) 777–784.

[22] H. Sakamoto, H. Hainu, and Y. Obata. Fluctuating forces acting on two square prisms in a tandem arrangement. *Journal of Wind Engineering and Industrial Aerodynamics* 26, (1987) 85–103.

[23] S. Luo and T. Teng. Aerodynamic forces on a square section cylinder that is downstream to an identical cylinder. *The Aeronautical Journal* 94, (1990) 203–212.

[24] C.-H. Liu and J. M. Chen. Observations of hysteresis in flow around two square cylinders in a tandem arrangement. *Journal of Wind Engineering and Industrial Aerodynamics* 90, (2002) 1019–1050.

[25] M. K. Kim, D. K. Kim, S. H. Yoon, and D. H. Lee. Measurements of the flow fields around two square cylinders in a tandem arrangement. *Journal of Mechanical Science and Technology* 22, (2008) 397.

[26] K. Tatsutani, R. Devarakonda, and J. Humphrey. Unsteady flow and heat transfer for cylinder pairs in a channel. *International Journal of Heat and Mass Transfer* 36, (1993) 3311–3328.

[27] A. Sohankar and A. Etminan. Forced-convection heat transfer from tandem square cylinders in cross flow at low Reynolds numbers. *International Journal for Numerical Methods in Fluids* 60, (2009) 733–751.

[28] W. Rodi, J. Ferziger, M. Breuer, and M. Pourquiée. Status of large eddy simulation: results of a workshop. *Journal of Fluids Engineering* 119, (1997) 248–262.

[29] X. Sun, C. Chan, B. Mei, and Z. Zhu. LES of convective heat transfer and incompressible fluid flow past a square cylinder. *Numerical Heat Transfer, Part A: Applications* 69, (2016) 1106–1124.

[30] S. Aus der Wiesche. Large-eddy simulation study of an air flow past a heated square cylinder. *Heat and mass transfer* 43, (2007) 515–525.

[31] C. J. Roy and M. F. Barone. Evaluation of detached eddy simulation for turbulent wake applications. Technical Report, Sandia National Laboratories 2005.

[32] F. Duchaine, M. Boileau, Y. Sommerer, and T. Poinsot. Large eddy simulation of flow and heat transfer around two square cylinders in a tandem arrangement. *Journal of Heat Transfer* 136, (2014) 101,702.

[33] X. Chen and H. Xia. A hybrid LES-RANS study on square cylinder unsteady heat transfer. *International Journal of Heat and Mass Transfer* 108, (2017) 1237–1254.

[34] P. R. Spalart. Comments on the feasibility of LES for wings, and on a hybrid RANS/LES approach. In Proceedings of first AFOSR international conference on DNS/LES. Greyden Press, 1997 .

[35] C. Dsouza et al. Effect of angle of attack and ow separation control on scramjet inlet using Hybrid RANS/LES. Ph.D. thesis, Indian Institute of Technology Hyderabad 2018.

[36] P. Spalart. Guide to detached-eddy simulation grids: NASA. Technical Report, CR-2001-211032 2001.

[37] M. Strelets. Detached eddy simulation of massively separated flows. In 39th Aerospace sciences meeting and exhibit. 2001 879.

[38] C. J. Greenshields. Openfoam user guide. *OpenFOAM Foundation Ltd, version* 3, (2015) 47.

[39] V. Gnielinski. Berechnung mittlerer Wärme-und Stoffübergangskoeffizienten an laminar und turbulent überströmten Einzelkörpern mit Hilfe einer einheitlichen Gleichung. *Forschung im Ingenieurwesen A* 41, (1975) 145–153.

[40] D. Lyn, S. Einav, W. Rodi, and J.-H. Park. A laser-Doppler velocimetry study of ensemble-averaged characteristics of the turbulent near wake of a square cylinder. *Journal of Fluid Mechanics* 304, (1995) 285–319.

[41] F. R. Menter, M. Kuntz, and R. Langtry. Ten years of industrial experience with the SST turbulence model. *Turbulence, heat and mass transfer* 4, (2003) 625–632.

[42] D. Sumner, S. Price, and M. Paidoussis. Flow-pattern identification for two staggered circular cylinders in cross-flow. *Journal of Fluid Mechanics* 411, (2000) 263–303.